ChemPhotoChem

Chemistry Europe
European Chemical Societies Publishing
ChemPhotoChem

RESEARCH ARTICLE OPEN ACCESS

Immobilization of Titanium Dioxide Ultrathin Films onto Porous Membranes via Atomic Layer Deposition for Photodegradation of Water-Borne Pollutants

Elisante M. Maloda[1,2] | Justine S. Nyarige[1] | Dmitry Busko[1] | Andrey Turshatov[1] | Bryce S. Richards[1,3]

[1]Institute of Microstructure Technology (IMT), Karlsruhe Institute of Technology (KIT), Eggenstein-Leopoldshafen, Germany | [2]Department of Physics, Mathematics and Informatics, Dar es Salaam University College of Education, Dar es Salaam, Tanzania | [3]Light Technology Institute (LTI), Karlsruhe Institute of Technology (KIT), Karlsruhe, Germany

Correspondence: Bryce S. Richards (bryce.richards@kit.edu)

Received: 16 January 2026 | **Accepted:** 29 January 2026

Keywords: atomic layer deposition | high-throughput screening | photocatalysis | photocatalytic membrane | titanium dioxide

ABSTRACT

Solar-driven generation of reactive oxygen species via photocatalytic membranes is a promising technology for the photodegradation of water-borne pollutants. Here, titanium dioxide (TiO_2) ultrathin films (11.9–28.05 nm) were grown on polytetrafluoroethylene (PTFE) and quartz-fiber filter (QFF) membranes via atomic layer deposition. The as-deposited (250°C) films were i) furnace annealed (300°C–1100°C) for 1 h or ii) via rapid thermal annealing (300–500°C) for 3 min. The presence of Ti coating onto/into QFF was confirmed, four times more than on PTFE. As-deposited TiO_2 films on QFF exhibited the crystalline phase of anatase, while no peaks were observed on PTFE. Films annealed on QFF at higher temperatures did not exhibit a mixed anatase-rutile phase, regardless of thickness. The films on QFF also exhibited significantly higher absorption of ultraviolet light (<400 nm) compared to the films on PTFE, which had limited absorption (<360 nm). Nonstoichiometric TiO_{2-x} films exhibited broad absorption from ultraviolet to the near infrared. The annealed films on QFF demonstrated high photocatalytic performance of about 88%–94% removal of methyl orange and 90%–97% for tartrazine 85 (compared to films on PTFE with 36% and 18%, respectively). The TiO_{2-x} films demonstrated improved performance compared to pure anatase TiO_2, paving the way for improved photocatalytic membrane performance.

1 | Introduction

The increase in micro-organic pollutants into both surface and ground-water bodies poses a serious threat to the availability of clean and safe drinking water [1]. Due to their small size and molecular weight, combined with their typically low concentrations in water, these pollutants pose significant challenges for many existing conventional wastewater treatment methods [2]. The use of modern filtration technologies based on pressure-driven membranes is not always capable of reliably retaining these pollutants, given their low molecular weight [3], plus the higher pressures required for nanofiltration or reverse osmosis also increases the energy demand of the process. Alternative technologies for eliminating such water-borne pollutants are based on advanced oxidation processes (AOPs) [4]. One such AOP, namely heterogeneous photocatalysis, has been mentioned as a potentially sustainable technique since the charge carrier excitation processes can be driven by solar energy [4]. The photogenerated carriers participate in redox reactions to produce in situ reactive oxidative species (ROSs)—such as superoxide radical anions ($O_2^{\bullet-}$), hydroxyl radicals ($^{\bullet}OH$), singlet oxygen ($^1O_2$), or hydrogen peroxide (H_2O_2)—that can mineralize a wide range of water-borne pollutants [5].

Among the inorganic metal oxide-based photocatalysts, titanium dioxide (TiO_2)—particularly in its anatase (A) crystalline phase

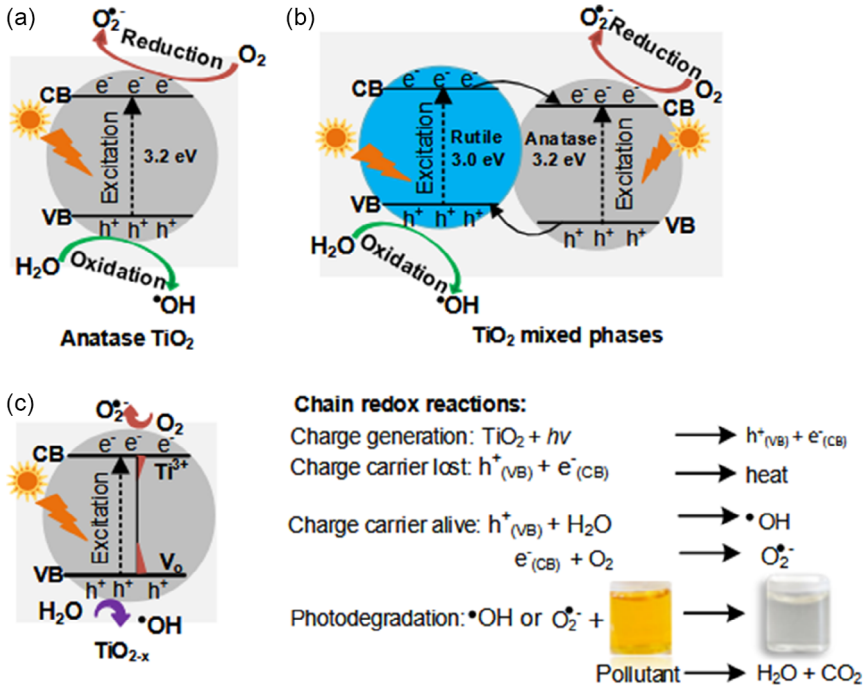

FIGURE 1 | Schematic illustrating the (a) electron–hole redox reactions for anatase, (b) anatase-rutile mixed phases for reducing charge carrier recombination, while (c) an interlocalized of oxygen vacancy (V_o) and titanium interstitial species (Ti^{3+}) between the VB and CB narrowing the bandgap, along with generating electron-hole pairs under light irradiation which then participate in reduction-oxidation reactions to produce ROS for photodegradation of the pollutants.

(Figure 1a)—has long been known to exhibit excellent photocatalytic properties [6]. This is because (i) the indirect bandgap of its anatase crystalline form exhibits a longer diffusion length of charge carriers [4, 7], (ii) the suitable potential edge position of the conduction band (CB) of about −0.42 eV and valence band (VB) of 2.87 eV for the oxygen-water redox reaction, respectively [4, 8], (iii) the low-cost and non-toxic oxide, and (vi) the excellent chemical and physical stability, thus affording a low degree of photocorrosion in aqueous solutions [9]. Despite these benefits, one major limitation of TiO_2 is its relatively wide bandgap of ∼3.2 eV (metastable A phase), which can absorb ultraviolet (UV) photons with wavelengths shorter than 388 nm, and the stable rutile (*R*) phase with a slightly lower (∼3.0 eV) direct bandgap, enabling activation with wavelengths less than 413 nm [10]. This exhibits a faster recombination rate, which limits the diffusion of generated carriers toward the surface, thus hindering the production of ROSs [4, 7, 11]. The TiO_2 photoactivation via UV light absorption accounts for only 4%–6% of the irradiance of the air-mass 1.5 global (AM1.5G) terrestrial solar spectrum, leaving the vast majority of visible photons unharnessed. If solar-driven degradation of water-borne pollutants could be achieved by immobilizing photocatalysts onto porous substrates to realize photocatalytic membranes, it would naturally offer a sustainable solution to an ever-growing problem.

Many different strategies have been explored to enhance the photocatalytic performance of TiO_2, including surface modifications via carbon nanostructures [12], A-R mixed phases [13], forming heterojunctions with other semiconductors [14], photosensitization [15], and using plasmonic materials [16]. In addition, bandgap engineering via realizing substoichiometric (TiO_{2-x}) materials [17] and doping with other metal ions [4, 18] were also demonstrated. Such approaches are designed to achieve either an improvement of charge separation or enhancing the visible light response, or both. Indeed, the A–R mixed phase and substoichiometric modifications have been identified as a pathway for boosting the photocatalytic activity of TiO_2 [19]. The enhanced performance of A–R mixed phases is attributed with favorable Fermi energy-level alignments and synergistic effects between the interfaces, which influences the flow of photoexcited electrons from the CB (−0.65 eV potential edge) of the R to the CB (−0.42 eV) of the A, while holes from VB (2.87 eV potential edge) of A to the CB of R (2.51 eV) as illustrated in Figure 1b, thus reducing the rate of charge recombination and increasing interfacial charge lifetime [20]. For instance, Degussa P25 nanoparticles have been highlighted as the best example of anatase–rutile TiO_2 composite with predominantly 75% A– 25% R mixture, which showed an excellent photocatalytic activity [21].

The reduction of stoichiometric TiO_2 to substoichiometric oxygen-deficient TiO_{2-x} (sometimes referred to as "black TiO_2") has been reported as a feasible way to improve the light absorption from UV to the visible range [22]. This enhancement is attributed to intrinsic electronic disorder and localized trap states of oxygen vacancies (V_o) and titanium interstitial species (Ti^{3+} and Ti^{2+}) from the oxidation of Ti^{4+} (as illustrated in Figure 1c). These features are associated with the creation of additional intrabandgap energy states below the CB edges ($Ti^{3+)}$ and above the VB edges (Vo), effectively narrowing the bandgap of TiO_2 (see Figure 1c). The formation of Ti^{3+} traps the photoelectron, inhibiting photoexited carrier recombination and improving the charge separation [17, 23]. For example, a study by Chen et al. [17] reported a bandgap of 1.54 eV for A-TiO_{2-x} nanoparticles and significant solar-driven photocatalytic activity during degradation of phenol and methylene blue. Shihao and co-workers [24] also claimed a wide range of light

harvesting—from UV to near-infrared (NIR)—with black A-TiO_2 (1.92 eV) nanoparticles and high performance on rhodamine B under visible light compared to white A-TiO_2 (3.1 eV).

The use of suspended TiO_2 nanoparticles in photocatalytic reactor water purification systems faces practical challenges, particularly in precipitating and recovering them from the slurry for reuse. To overcome these drawbacks, the idea of immobilizing TiO_2 onto and into the porous structure of a membrane has emerged, which can be either polymeric or inorganic membranes, and the coating could be formed from TiO_2 nanoparticles [25] or a continuous TiO_2 film [26]. Recent work from our group has demonstrated that when the photocatalyst is immobilized with porous membranes, then fast photodegradation kinetics are observed. For example, Berger et al. [27] reported a photocatalytic rate of 2.30×10^{-7} mol/m^2 s using TiO_2 -coated anodized aluminum oxide membranes, while Lyubimenko et al. [28] achieved a rate of 2.25×10^{-6} mol/m^2 min using organic photosensitizers coated onto polyvinylidene fluoride membranes.

Among the TiO_2 film preparation methods, atomic layer deposition (ALD) is widely recognized as an excellent technique for growing ultrathin (5–10 nm-thick) layers over the large surface areas of the substrate [29]. ALD offers accurate thickness control, very good conformal coverage of high-aspect ratio substrates (including porous materials), as well as uniform growth for excellent reproducibility and scalability [30]. With these benefits, ALD was chosen as an optimal method for the coating of TiO_2 films to the membranes in this work.

The film thickness is one of the major parameters that strongly influences the absorption of photons and interfacial charge transfer in photocatalytic reactions [31]. This is due to the fact that enhancement of photocatalytic performance is highly attributed to balancing the film thickness, the penetration depth of photons, and the diffusion length of photogenerated charge carriers from the bulk to the surface, where the ROS can drive photocatalytic reactions [32]. While numerous studies have reported the dependance of photocatalytic activity on TiO_2 film thickness, a comprehensive correlation between film thickness and photocatalytic efficiency has not been well-documented among researchers, particularly for the ultrathin film thicknesses. For example, Kääriäinen et al. [33] demonstrated higher photocatalytic performance with 15 nm-thick A-TiO_2 films grown on soda lime glass using ALD compared to thicker films of 65, 130, and 260 nm of A–R mixed phases, which exhibit fast recombination of the photogenerated carriers due to R-dominant. The study of Levchuk et al. [34] reported lower performance with 100 nm-thick A-TiO_2 films coated onto an aluminum foam substrate via ALD during the photodegradation of phenol. Vilhunen and co-workers [35] highlighted the low removal efficiency of salicylic acid with 46 nm-thick A–R (dominant) TiO_2 films grown on silica substrates by ALD.

Despite several reports of immobilizing ALD TiO_2 films on various nonporous supports, membrane substrates have gained attention since they possess a large specific surface area-to-volume ratio to accommodate adequate photocatalytic materials [35]. A comprehensive study of the ultrathin TiO_2 films (10–30 nm thickness) immobilized onto membranes via the ALD method for the photocatalytic degradation of pollutants in water has not been extensively evaluated. Berger et al. [27] reported removal efficiencies of methylene blue in flow-through single pass, with a range of 2–15 nm thickness of A-TiO_2 thin films coated on anodized aluminum oxide ceramic porous membrane via thermal ALD. The study of Lotfi et al. [36] demonstrated different removal of steroid hormones in continuous single-pass flow using A-TiO_2 nanoparticles (10–30 nm) immobilized on polyethersulfone membranes. Hatat-Fraile et al. [25] investigated the pristine and doped A-TiO_2 nanoparticles coated on quartz fiber filters (QFF) via the sol–gel dip-coating technique in the photodegradation of acid orange 7 dye with dead-end filtration.

The present study focuses on depositing ultrathin TiO_2 films on two different types of membranes, first, QFF and, secondly, polytetrafluoroethylene (PTFE) membranes using thermal ALD for the photocatalytic degradation of two photostable anionic dyes, methyl orange (MO) and tartrazine 85 (T85) dye aqueous solution using in operando characterization in a batch reactor, fast screening photocatalytic reactor system (FaS-PhoReS) as highlighted in our previous work [37]. These membranes were chosen because they are: (i) flexible and robust, unlike the brittle AAO membranes used previously [27]; (ii) they are commercially available in sheet form; and (iii) offer very contrasting temperature limits. Specifically, the QFF substrates allowed for high-temperature annealing—and standard furnace annealing (FA) in a variety of gas ambients performed at up to 1100°C—whereas the PTFE membranes have a recommended maximum temperature of 260°C. This greatly limits the possibility of realizing a polycrystalline TiO_2 ultrathin film at such low temperatures. In an attempt to achieve a crystalline TiO_2 film on low-temperature substrates such as polymeric membranes, several approaches have been used, such as microwave furnace [38], plasma-enhanced [39], and laser irradiation [39], and rapid thermal annealing (RTA), which realizes fast temperature increment in a short time, as highlighted in Table 1. In this research, the RTA technique will be employed via voltage settings to achieve extremely rapid increases in temperature for 3 min, reducing the required annealing duration from hours (typical for FA) down to a duration of a few minutes.

Thus, this work aims to develop and test the solar-driven photocatalytic membranes via: (i) conformally depositing ultrathin TiO_2 film, 11–28 nm-thick onto/into the porous polymeric (PTFE) and inorganic membranes (QFF), (ii) investigating the possibility of annealing TiO_2 films on the PTFE substrates;

TABLE 1 | Summary of the results achieved through RTA for the crystallization of TiO_2 thin films on low-temperature polymeric substrates.

RTA conditions	Resulting phase	Key outcomes	Ref
400°C, 1 min	Anatase	Improved crystallinity exhibited high photocatalytic activity.	[40]
850°C, 1 min	Rutile	Improved crystallinity exhibited low photocatalytic performance.	
1200°C–1300°C, 1–10 s (150°C/s)	Anatase–rutile mixed	Improved crystallinity, photodegradation not tested.	[41]
600°C, 1 min (600°C/min)	Anatase-rutile mixed	High crystallinity, photodegradation not tested.	[42]

(iii) exploring the influence of annealing temperatures and substrate choice on film crystallinity and the A-R phase transformation; and (iv) creating visible light–active reduced TiO_{2-x} films through forming-gas annealing (4% hydrogen in 96% argon).

Overall, this article addresses four specific research questions: (i) How does varying the thickness of as-deposited ALD TiO_2 ultrathin films influence crystallinity and photocatalytic performance? (ii) How do both the annealing temperatures and substrate choice influence the crystallinity and A–R phase transformation of the TiO_2 ultrafilms? (iii) Which of the TiO_2 ultrathin films annealed at various temperatures exhibits superior photocatalytic degradation of photostable dyes under simulated sunlight? (iv) Which among the titanium oxide films (TiO_2 or TiO_{2-x}) coated onto QFF substrates exhibits the highest removal efficiency when photodegrading the photostable dyes under simulated terrestrial sunlight?

2 | Materials and Methods

2.1 | Preparation of Substrates

Four different substrates were employed, two different types of planar (non-porous) substrates for characterization purposes only: (i) fused silica glass (Fused Quartz JGS2) and (ii) double-sided polished *p*-type 100 silicon (Si) wafers (International Wafer Service, USA) as well as two different porous membranes: (iii) 300 μm-thick QFF (QFF: Advantec Sterlitech, QR-100, Germany), chosen due to their excellent chemical resistance, low light absorption, and thermally stability up to 1100°C; and (iv) 28 μm-thick polytetrafluoroethylene (PTFE) membranes (Fluorotex-G-400−0.2-FG, Kögel Filter GmbH, Germany) that can withstand a maximum temperature of 260°C. The thickness of the membranes was measured using a height gauge (Mitutoyo 952625, Japan). The QFF and PTFE membrane supports were cut using scissors into several pieces of 30 × 150 mm from larger rectangular sheets (203 × 254 mm for QFF and 500 × 300 mm for PTFE) for the deposition process without additional cleaning.

2.2 | Deposition of ALD TiO_2 Films

The pristine TiO_2 ultrathin films were grown on QFF, PTFE, fused silica, and Si substrates using an ALD reactor (Picosun R-200, Finland) in thermal mode, with 300–700 cycles in 100-cycle increments. Titanium tetrachloride ($TiCl_4$, 99.9%, SAFC Hitech, USA, CAS: 7550-45-0) was used as the Ti source and deionized water as the oxygen source to grow TiO_2 films at a deposition temperature of 250°C. Both precursors were sealed into two separate stainless steel cylinder bubblers to achieve TiO_2 films via a hydrolysis reaction. Ultrahigh-purity nitrogen (N2 99.999%) was used as a carrier gas to transport the precursor molecules into the chamber and to remove redundant ligands. During deposition, both bubblers were kept at room temperature (23°C) to ensure sufficient vapor pressure. For a single deposition run of TiO_2 films, a total of 12 substrates were loaded into the ALD chamber: two pieces of Si (10 × 10 mm), eight pieces of fused silica (20 × 20 mm), one QFF sheet (30 × 150 mm), and one PTFE sheet (30 × 150 mm). The deposition chamber was evacuated for 2 h to achieve a pressure of 9 hPa. One ALD subcycle consisted of a 0.1 s pulse of $TiCl_4$ to be adsorbed onto the substrate to form Ti, followed by 9 s of purging with N_2 to evacuate unreacted $TiCl_4$, then a 0.1 s pulse of H_2O to react with Ti, and 13 s of purging with N_2 to remove byproducts such as CO_2, H_2O, and HCl. The process was repeated sequentially, subcycles of $TiCl_4$ / N_2 / H_2O / N_2, to achieve monolayer growth of TiO_2 on the substrates, with the number of cycles ranging from 300 to 700. After the deposition period, the ALD was switched off and left to cool to room temperature. The TiO_2-coated membrane sheets were then cut into three sizes—10 × 10 mm (surface morphology testing), 10 × 20 mm (optical characterization), and 20 × 20 mm (photocatalytic performance)—followed by postannealing.

2.3 | Postdeposition Annealing of TiO_2 Films

Three different annealing systems were used in this work: (i) a photonic curing system (Novacentrix Pulse-Forge 1200) was employed primarily for achieving rapid heating rates (rapid thermal annealing) for the low-temperature PTFE substrates; (ii) a muffle furnace (Thermo Concept KLS 05/11) was used for FA in air; and (iii) a quartz tube furnace (GSL-1500X, MTI Corporation, USA/China) was used for annealing in forming gas (4% hydrogen in 96% argon). Two temperature regimes were investigated: (i) the lower temperature range of 300°C–500°C (both FA for 1 h and RTA for 3 min) was intended to investigate the effect of temperature on the phase transformation of the as-deposited amorphous TiO_2 ultrathin films into the crystalline anatase phase and (ii) the higher-temperature range of 600°C–1100°C was chosen to realize A–R mixed phases. The as-deposited TiO_2 ultrathin films coated onto high-temperature-stable substrates (QFF, along with silica and Si) were FA at a heating rate of 5°C min^{-1} from 300°C to 1100°C in air for 1 h under the same conditions. The TiO_2 films on PTFE were only annealed at 300°C in FA due to instability at high temperatures. For RTA, the system was first simulated under the specified settings of voltage, pulse length, and number of pulses, which corresponded to the required temperatures. Then, TiO_2 films coated onto all substrates were annealed from 300°C to 500°C (in 50°C steps) for 3 min in air. It was observed that at RTA temperatures greater than 500°C, the PTFE membrane started to melt. As-deposited TiO_2 films were coated on QFF and underwent FA in a forming gas atmosphere to produce reduced TiO_{2-x}. Table S1 summarizes the deposition and annealing conditions of all samples, while Table S2 highlights RTA voltage settings versus achieved annealing temperatures.

2.4 | Characterization of TiO_2 Films

The crystallinity of TiO_2 films on all substrates was investigated using an X-ray diffractometer (XRD, D2 Phaser, Bruker, Germany) with CuKα radiation (λ = 0.154184 nm, scan rate = 0.02°/s, 2θ = 10°–80° range). The possible orientations of TiO_2 patterns—both A and A–R mixed phase—were compared with International Centre of Diffraction Data (ICSD) 9852 and 16636, respectively. The thickness of the TiO_2 films was measured on fused silica substrates using X-ray reflectometry (XRR, D8 Discover, Bruker, Germany). The film thicknesses on the QFF and PTFE membranes were assumed to be similar to those measured on the planar fused silica substrates since all the samples were deposited under the same conditions and

environment. A scanning electron microscope (SEM: Zeiss Supra 60VP, Germany) was used to examine the uniformity and surface morphology of the TiO_2 films on the QFF and PTFE membranes, while the elemental compositions were analyzed via energy-dispersive X-ray (EDX) spectroscopy (EDX, Vega 3, Tescan, Czech Republic with XFlash 610 M detector, Bruker, USA) mounted onto the SEM. The TiO_2 film roughness on the QFF and PTFE membranes was measured using atomic force microscopy (AFM: CP-II Scanning Probe Microscope Instruments) and examined in terms of mean surface roughness, S_a (nm), peak height, S_z (nm), and root mean square height, RMS (nm). The optical absorption of the TiO_2 films on the QFF and PTFE membranes, as well as fused silica substrates, was measured using an integrating sphere setup in the UV–vis–NIR spectrophotometer (Agilent Cary 7000, USA) from 300 to 1000 nm. The TiO_{2-x} and pure TiO_2 films coated on silica were then directly fixed into the holder and mounted in the middle of an integrating sphere. In contrast, the pristine and TiO_2-coated QFF and PTFE membranes were placed inside a quartz cuvette (4 × 1 cm) filled with deionised (DI) water that was then mounted in the center of the integrating sphere. This ensures that all scattered light in the porous samples is accounted for in the same operational conditions as during photocatalytic experiments.

2.5 | Photodegradation Prototype Experiment

The photocatalytic performance of the TiO_2 and TiO_{2-x} ultrathin films was evaluated via the degradation of two dye aqueous solutions, methylene orange (MO) and tartrazine 85 (T85), using FaS-PhoReS, which enables in operando photodegradation of up to 32 wells containing different photocatalytic materials and/or optically active pollutants under metal halide (1200 W MH-lamp, Osram, Germany) full simulated spectrum (Figure 2, magenta curve) from a climate chamber (DM340-CS-R, ACS, Italy). The full spectrum of the MH lamp allowed uniform irradiance of 100 mW/cm^2 over the 32 wells of the tray sample. The decrease in dye concentration was monitored by a UV–vis–NIR spectrometer coupled to the system by measuring light intensity through well-contained aqueous solutions and TiO_2 films. The recorded intensity was used to determine the amount of light absorbed by the dye molecules. The preparation of the dye aqueous solutions and the FaS-PhoReS experiments was conducted similarly to those in a previous work [37].

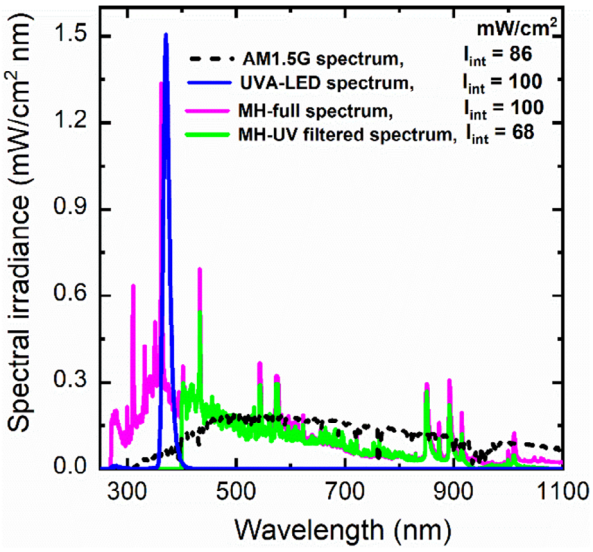

FIGURE 2 | The spectral irradiance of the solar simulator metal halide lamp (full spectrum – magenta and UV filtered – green) and UVA-LED (blue) used in this work compared to the AM 1.5G terrestrial solar spectrum (black). I_{int} represents the integrated light intensity available in the respective wavelength region.

Briefly, before photocatalytic experiments were conducted, 20 mL of DI water was disseminated in 31 wells and irradiated using a metal halide lamp for 120 min, while well 32 was blacked out (0% light transmission) for all the experiments, both for the baseline correction during the data analysis. For photocatalytic experiments, 20 mL of 0.01 mM MO aqueous solution was consistently dispensed into 31 wells. One well without TiO_2 was reserved for the control experiment (photolysis), and 30 wells were loaded with TiO_2 ultrathin films, both as-deposited and annealed, coated onto the QFF and PTFE membranes. The sample tray was left in the dark for ~ 15 min before turning the solar simulator on. After the 360 min experiment, the MO aqueous solutions were removed, and the TiO_2 ultrathin films-coated membranes were rinsed with DI water to remove contaminated dye molecules and then dried at ambient temperature for 12 h for the repeat experiment. Each photodegradation experiment was performed in triplicate to ensure the consistency of the results and the reusability of the samples. Similar procedures were repeated for the 0.01 mM T85 solution using a different set of similar TiO_2 ultrathin films. For testing the photocatalytic degradation of TiO_{2-x}-coated QFF substrates, the standard (UV-rich MH-full spectrum) solar simulator was employed and MH-UV filter (Figure 2 – green curve) formed from a 10 mm-thick polycarbonate sheet that blocked all light below 400 nm.

Furthermore, as shown in Figure 2 of the irradiation sources, MH-UV-filtered (green curve - below 400 nm) and UVA (blue curve) illumination from a 365 nm light-emitting diode (LED, iSFL XS, Opsytec Dr. Gröbel, Germany) were also employed to check whether the photocatalytic performance of TiO_2 and TiO_{2-x} photocatalytic membranes (PCMs) under simulated MH-full spectrum (magenta curve) was partially attributable to dye photosensitization, as previously observed by Ohtani et al. [43] and Rochkind et al. [44]. The 365 nm UVA-LED was fixed at a height of 11 cm above the sample wells to achieve an average light intensity of 98 ± 2 mW/cm^2, measured using a radiometer (RMD Model 814401, Opsytec Dr. Gröbel, Germany) connected to a sensor (UVX-A-B, Opsytec Dr. Gröbel, Germany). The height was adjusted to achieve an average intensity of 100 mW/cm^2, which is comparable to 100 mW/cm^2 of the MH-full spectrum (280–1100 nm) and roughly corresponding to 86 mW/cm^2 integrated irradiance from 300 to 1100 nm of the air-mass (AM) 1.5 global (G) terrestrial solar spectrum (black curve) [45]. The 68 mW/cm^2 of MH-UV filtered in the 400–1100 nm range. The annealed (500°C) 700 cycles TiO_{2-x} and TiO_2 thin films-coated QFFs were placed in the wells containing 20 mL of 0.01 mM initial concentration of MO and T85 dye aqueous solution for a 360 min period of irradiation. To test the adsorption degradation in the dark, the TiO_2 thin films coated on QFF (600°C) were immersed in 20 mL of MO and T85 aqueous solutions in the well were performed for a period of 6 h. At an interval of 1 h, 2 mL aliquot of each sample was collected from the 20 mL and placed into a quartz glass cuvette for the

absorbance measurement (300–800 nm) and replaced after measurement. The photodegradation efficiency was evaluated by measuring the absorbance of the aliquot sample using a UV–vis–NIR spectrophotometer (Agilent Cary 7000, USA).

3 | Results and Discussion

3.1 | TiO_2 Thin-Film Characterization: Thickness and Crystallinity

The thicknesses of as-deposited (250°C) TiO_2 films (Table 2) on the planar fused silica substrate as a function of the number of ALD cycles were determined using XRR. The growth rate of the films on fused silica substrates was calculated to be 0.04 nm/cycle. The results reveal a significant increase in thickness for the as-deposited films as a function of ALD cycles (see Figure S1). The annealing temperatures were found to have a negligible influence on the film thickness, as shown in Table S3; thus, no further XRR determination of thickness for other ALD cycles was performed. A slight decrease in the thickness of the annealed TiO_2 films is ascribed to the densification of the thin film and a decrease in impurity concentration of chlorine from the $TiCl_4$ precursor, and hydrogen from the water oxidant, which often declines at elevated temperatures due to thermal decomposition of ligands [46, 47].

To confirm the crystal phase structures of the TiO_2 ultrathin films grown on QFF and PTFE membranes (also on fused silica and Si as reference) from 300 to 700 ALD deposition cycles, XRD measurements were carried out. Figure 3 illustrates XRD patterns of the as-deposited and annealed TiO_2 films onto QFF and PTFE membranes, along with ICDS anatase (9852) patterns for reference. From Figure 3a, the as-deposited TiO_2 on QFF indicates a significant increase in A peak intensity as a function of film thickness. It is worth mentioning that the growth rate of TiO_2 on QFF is likely due to the reactive sites of hydroxyl groups that contribute to the increase in deposition rate. These create reaction mechanisms for the precursor in ALD reactions to produce films. No A peaks were detected for the as-grown TiO_2 on PTFE (Figure 3b), regardless of the thickness. This is likely due to the hydrophobic nature of PTFE, which lacks hydroxyl reactive groups, suppressing the ALD hydrolysis reaction and lowering the growth rate of TiO_2 [48]. The low growth rate of PTFE membrane was confirmed by growing 700 cycles TiO_2 thin films (250°C) onto a planar PTFE substrate. The growth rate is less than half (0.017 nm/cycle) compared to that on fused silica and Si, with the film remaining amorphous (Figure S2) even after FA at 300°C. The as-deposited films on fused silica and Si (see Figure S3a,b) only exhibited an A peak from 500 cycles, likely because the effective volume of the deposited film is significantly less than that deposited into the porous membranes. Shi et al. [49] also observed that on Si substrates, the anatase phase was only present for TiO_2 films deposited with more than 400 cycles.

TABLE 2 | Thickness of as-deposited (250°C) TiO_2 ultrathin films on fused silica substrates measured using XRR.

ALD cycles	300	400	500	600	700
Thickness (nm)	11.90	15.60	20.30	23.87	28.05

Figure 3c–f presents the XRD patterns of the polycrystalline anatase TiO_2 ultrathin film (700 cycles) deposited on QFF and PTFE after postannealing at the lower temperature range of 300°C–500°C via both RTA and FA. The TiO_2 films coated on QFF membrane, both annealed via RTA (Figure 3c) and FA (Figure 3e), displayed a strong anatase peak at 25.6°, corresponding to the (101) plane, as well as other weaker reflections corresponding to the (103), (004), (112), (200), (105), and (211) planes. These results matched well with ICDS reference patterns of anatase and also aligned well with the report of Badovinac et al. [50], who used ALD TiO_2 films on quartz glass, and Hatat-Fraile et al. [25] TiO_2 nanoparticles on QFF. The XRD peak intensities increased with annealing temperatures, both for FA and RTA samples. The TiO_2 films on PTFE membrane (Figure 3d,f) indicate a very weak (101) anatase peak that increases very slightly as the annealing temperature rises from 300°C to 500°C in RTA and at 300°C in FA. In addition, at temperatures >300°C (FA) and >500°C (RTA), respectively, the PTFE membranes exhibited signs of melting (see Figure S14). For completeness, the XRD patterns of the as-deposited and annealed (RTA and FA) TiO_2 films for all other thicknesses (600–300 cycles) and coated onto all substrates—QFF, PTFE, silica, and Si—are given in Figures S4–S12. For the TiO_{2-x} films (500 cycles), the XRD diffractograms are presented in Figure S13a,b, with a clear anatase phase being presented on QFF and a smaller (101) anatase plane being observable on silica substrates.

Further, TiO_2 ultrathin films (11.9–28 nm thick) were annealed at elevated temperatures from 600°C to 1100°C to investigate the transformation of the as-deposited films into A–R mixed phases. The findings indicate that (Figures S4–S11) the TiO_2 films on QFF exhibit an increasing crystallinity, but the A does not transform into R, even despite the high annealing temperatures. Thus, the A structure is retained, even though the thermodynamic transformation to R is known to typically occur at temperatures above 650°C [51]. This retarded phase change is likely due to the ultrathin layer of TiO_2 grains coated on the QFF fibers, which limits the coalescence and growth into larger structures for the A–R phase transformation [52]. A similar trend has been reported in the literature for ALD TiO_2 thin films deposited onto QFF for application in solar cells [51]. In contrast, an A–R mixed phase is observed in the TiO_2 films deposited onto Si for annealing temperatures above 800°C. In a final attempt to produce an A–R mixed phase on the QFF, a lower ALD deposition temperature of 150°C was used with 700 cycles and then underwent FA at 1100°C. Again, under these conditions, while an A–R mixed phase was observed on the Si substrate, none could be detected on the QFF. These findings indicate that the transformation of amorphous and anatase TiO_2 ultrathin films into A–R mixed phase is not only temperature dependent, but also influenced by the film thickness and nature of the substrate employed. The results are in agreement, where 17–20 nm-thick TiO_2 films deposited onto Si substrates via ALD exhibited A–R mixed phase after annealing at 800°C–1000°C [49].

3.2 | TiO_2 Thin-Film Characterization: Morphology

To investigate the surface uniformity of the TiO_2 ultrathin films, two samples, the films deposited with 700 cycles and annealed via FA at 1100°C (QFF) and RTA at 500°C (PTFE), were chosen

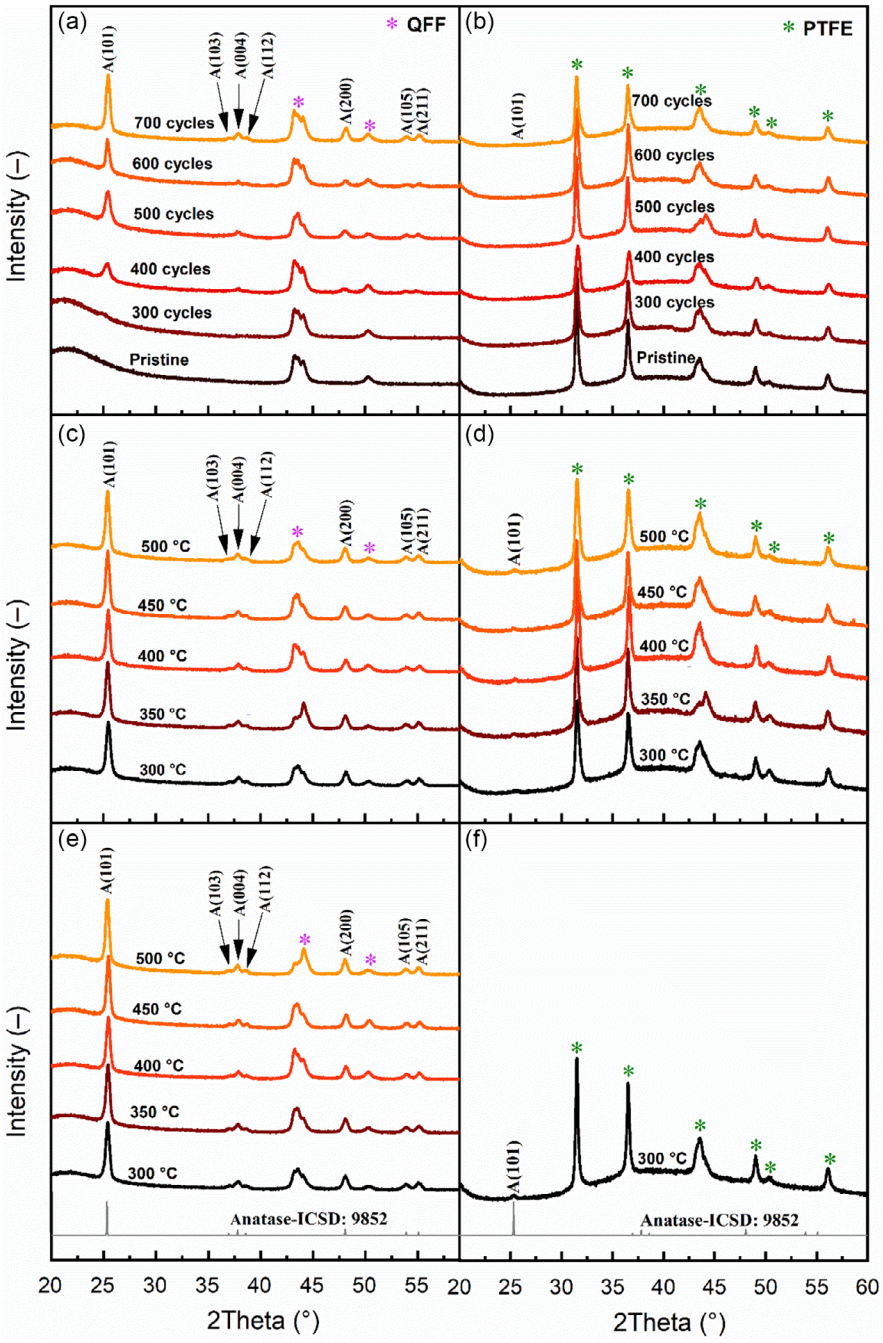

FIGURE 3 | XRD patterns of the as-deposited (250°C) TiO_2 ultrathin films on (a) QFF and (b) PTFE from 300 to 700 cycles, as well as the pristine (uncoated) membranes. The XRD patterns of 700 cycles TiO_2 ultrathin films that have undergone RTA, on (c) QFF and (d) PTFE, as well as FA samples, again, on both (e) QFF and (f) PTFE. For clarity, the XRD reflections resulting from the QFF (*) and PTFE (*) substrates are marked.

for SEM analysis. Figure 4 shows the surface morphology of the QFF substrate, before (pristine, Figure 4a) and after coating with TiO_2 and undergoing FA at 1100°C (Figure 4b). The pristine QFF exhibits a smooth surface of the microfibers, whilst the TiO_2-coated QFF has a granular structure attached to the surface of the microfibers. The SEM image of coated QFF revealed no agglomeration of TiO_2 on the microstructure of the fibers. The SEM images for the pristine PTFE membrane (Figure 4c) and after coating with TiO_2 (700 cycles) annealed at 500°C in RTA (Figure 4d) appear very similar. Although a small anatase peak was evident in the XRD analysis (Figure 4f), this cannot be seen here. For comparison, the SEM images of 700 cycles TiO_2 films grown on fused silica (Figure S15) indicate a homogeneous and compact structure covering the entire surface of the substrate without pinholes, which agrees with ALD-TiO_2 SEM images reported by Birnal et al. [53] and Szindler et al. [54] In addition, Figure S15a–c indicates an increase in crystallite appearance as a function of temperature due to agglomeration of several grains. EDX cross-sectional analysis was employed to investigate the depth profile of the TiO_2 coating and how this extends into the internal pore structures of the 300 µm-thick QFF and 280 µm-thick PTFE membranes. A linescan of the Ti counts from the EDX signal is plotted in Figure 4e, where 0 µm represents the top surface of the membrane and ~300 µm the bottom. There are

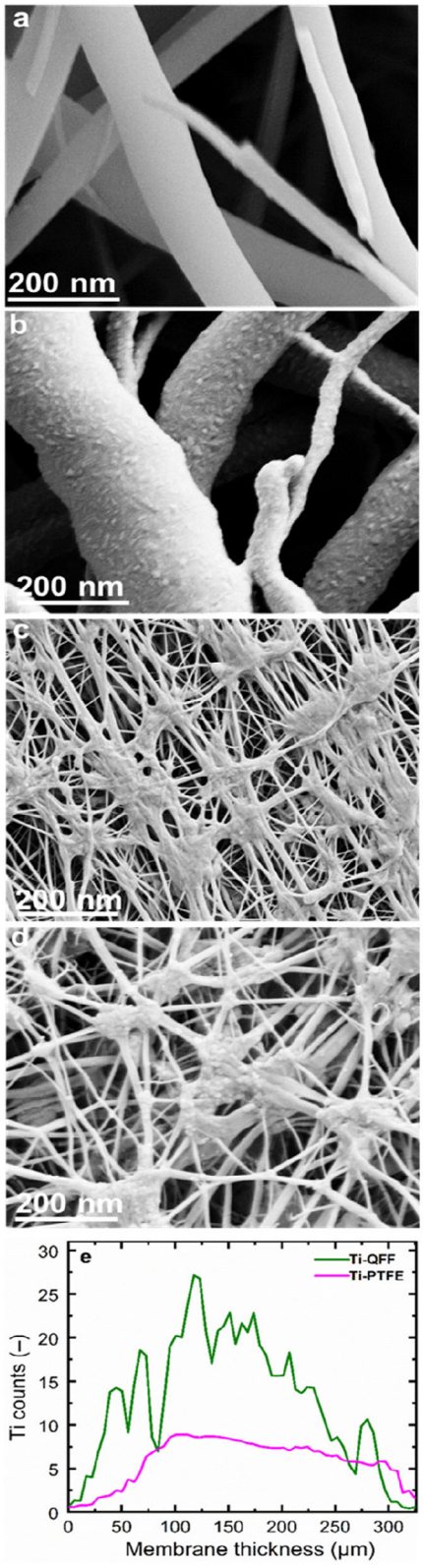

FIGURE 4 | Plan-view SEM images of the surface morphologies of: (a) uncoated (pristine) QFF and (b) TiO_2-coated QFF membranes (700 cycles) annealed at 1100°C via FA, (c) uncoated (pristine) PTFE and (d) TiO_2-coated PTFE (700 cycles) annealed at 500°C via RTA; (e) the titanium (Ti) counts from EDX line scans performed over the cross section of both photocatalytic membranes (700 cycles TiO_2) on QFF (FA at 1100°C) and PTFE (RTA at 500°C).

two key observations here. First, the amount of Ti reaches a maximum toward the middle of the membrane and is significantly lower at the top and bottom surfaces. This is not expected to be an artifact of the EDX measurement, since its resolution is ~3 μm for the 15 keV electron beam that was used for these samples, which is much smaller than the membrane width. Secondly, the Ti counts are four times higher on the QFF sample compared to the films on PTFE, confirming that TiO_2 coating did occur on the hydrophobic PTFE, but at a significantly lower growth rate than on the hydrophilic QFF surface.

To examine the surface roughness of the TiO_2 layers, the thickest film (700 cycles, 28.05 nm) coated onto QFF was chosen for AFM analysis using a scanning area of 1.2×1.2 μm and quantified by mean surface roughness, S_a (nm), peak height, S_z (nm), and root mean square height, RMS (nm). Figure S16a indicates the AFM scanned area of the QFF fiber coated with TiO_2, while Figure S16b–d displays the 3D AFM roughness topography of the as-deposited and annealed TiO_2 ultrathin films coated on QFF. Figure S16b shows the uniform grains and smooth surface area of a fiber-coated TiO_2 before annealing. The results reveal the following values: $S_a = 1.32$ nm, $S_z = 21.5$ nm, and RMS = 1.74 nm. The film annealed at 500°C (see Figure S16c) revealed an increase in surface roughness ($S_a = 3.71$ nm, $S_z = 69.8$ nm, RMS = 5.22 nm), indicating the growth of the crystallites as a result of agglomerated grains. At an elevated temperature of 1100°C (see Figure S16d), the highest values of 15.6 nm (S_a), 97.0 nm (S_z), and 18.7 nm (RMS) TiO_2 films were demonstrated. The AFM topography indicates a rough surface with dense columnar-shaped crystals (Figure S16d).

3.3 | TiO_2 Thin-Film Characterization: Optical Properties

To investigate the UV–vis response to the TiO_2 ultrathin films grown on both QFF and PTFE membranes, the optical absorbance was measured. Figure 5 displays the optical absorbance of the 700 cycles TiO_2 films coated onto (i) QFF, before and after FA at 300°C–1100°C (Figure 5a); (ii) PTFE, before and after RTA at 300°C–500°C annealing (Figure 5b); as well as (iii) reduced TiO_{2-x} films to the QFF that underwent FA in forming gas for 1 h at 500°C (Figure 5c) covering the UV–vis–NIR range. The pristine QFF and PTFE exhibit an absorbance of less than 0.1.

As shown in Figure 5a, there is a noticeable increase in UV absorbance from 0.83 (250°C) to 1.08 (700°C), both below the absorption edge of 395 nm, and a slight increment beyond it up to 1.15 at 1100°C, with the absorption edge shifting down to 370 nm. It is found that there was an increase in integrated absorbance (integrated between 300 and 450 nm) as function of temperature from 54.50 (250°C), 58.78 (300°C), 64.87 (500°C), to 67.33, (700°C) and a decrease to 65.25 (900°C), 57.23 (1000°C), and 54.89 (1100°C). The variation in integrated absorbance is attributed to differences in maximum absorption and shifting in the absorption edge.

The TiO_2 films coated on PTFE (Figure 5b) follow a similar trend of increase in absorbance as a function of annealing temperature. As can be observed, the as-deposited film (250°C) absorbs a maximum of 0.26 below the absorption edge of 350 nm with an integrated absorbance of 13.65 extended to about 0.29 (300°C) up to 0.45 (500°C) with RTA with an integrated absorbance of 15.71

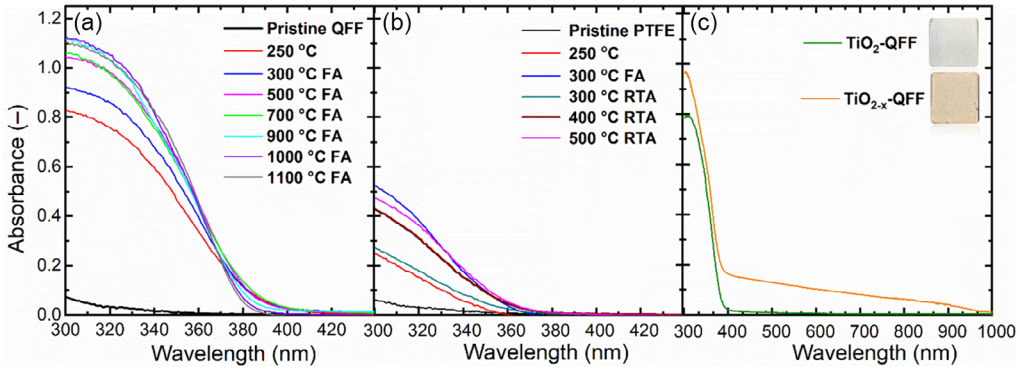

FIGURE 5 | UV–vis–NIR absorption spectra of pristine QFF, PTFE, as-deposited, and annealed (FA and RTA) TiO_2 ultrathin films (700 cycles) coated on (a) QFF, (b) PTFE, and (c) absorbance comparison between TiO_2 versus TiO_{2-x} ultrathin films on QFF, both undergoing FA at 500°C, but the former in air and the latter in forming gas (4% H_2 and 96% Ar).

and 20.84, respectively, while maximum of 0.48 at 300°C (FA) with the integrated absorbance of 22.71. The results indicate that TiO_2 films onto QFF absorb light four times as much as those coated onto the PTFE. This is attributed to the amount of TiO_2 on membranes, as evident from XRD and SEM analysis. In addition, the absorbance of the as-grown and annealed (RTA and FA) TiO_2 films for all other thicknesses (300–600 cycles) coated on the QFF and PTFE is illustrated in Figures S17–S20 (700 cycles).

Figure 5c illustrates the comparison of the absorbance between the pure A-TiO_2 and reduced A-TiO_{2-x} films coated onto QFF substrates—both at 700 cycles and annealed at 500°C (see also Figure S21). The observation revealed a clear change in color from the normal white appearance of the QFF membrane (TiO_2 films annealed in air remain stoichiometric and do not change the color) to the light-brown color of the substoichiometric TiO_{2-x} resulting from forming gas annealing. The brown color formation is likely due to the absorption tail in the spectrum of TiO_{2-x}, which is associated with the presence of oxygen vacancies. The TiO_2 exhibits absorbance of 0.80 at 300 nm and is negligible at wavelengths greater than 400 nm. In contrast, the TiO_{2-x} sample exhibits a high absorbance in the UV (maximum of 0.99) as well as a significant broadening of the light absorption, extending through the visible out as far as 1000 nm. The large UV absorption peak for both TiO_{2-x} and TiO_2 is ascribed to the intrinsic bandgap absorption of crystalline A [53], while the extension of light absorption into the vis–NIR range could be attributed to the presence of localized midbandgap states of oxygen vacancies at the upper level of the valence band [23].

The optical bandgaps (E_g) of the TiO_2 and TiO_{2-x} films were evaluated using the Tauc relation, illustrated in Figure S22. The calculated bandgaps are in the range of: (i) 3.20–3.26 eV for TiO_2 films on QFF, comparable with the bandgap of anatase reported by Hatat-Fraile et al. [25], Arlos et al. [55], and Kim et al. [56]; (ii) 3.4–3.6 eV for TiO_2 films on PTFE, which agrees with the expected bandgap of amorphous TiO_2 [49]; and (iii) the TiO_{2-x} film has a value of 3.10 eV (Table S4). The latter value agrees with the 3.09 eV bandgap for TiO_{2-x} reported by Wang et al. [57] and Bazzanella et al. [58]. However, it should be emphasized that the localized defect states of oxygen vacancy states (which remain unknown) could result in greatly varying values.

3.4 | TiO_2 PCMs: Photodegradation Analysis Using FaS-PhoReS

The photocatalytic performance of the TiO_2-coated QFF and PTFE-based PCMs was evaluated using the ratio of the dye absorbance (A_t/A_o), which is proportional to the concentration ratio (C_t/C_o) at a particular time of irradiation, where A_o and A_t are the integrated absorbance at $t = 0$ min and at any given time interval t min, respectively. The integrated absorbance (A) was evaluated over a 330–580 and 320–510 nm wavelength range, covering the absorption spectrum of the two chosen dyes, MO and T85, respectively, using Equation (1):

$$A = \sum_{A_{\lambda_{min}}}^{A_{\lambda_{max}}} (a_t) \quad (1)$$

where a_t is the absorbance of each band with respect to time intervals, while $A_{\lambda_{min}}$ and $A_{\lambda_{max}}$ are the absorbance at the minimum and maximum wavelengths of the spectra.

Figure 6 demonstrates the time evolution of absorption spectra of MO and T85 dyes dissolved in water at a concentration of 0.01 mM due to photocatalysis with TiO_2 PCMs based on QFF and PTFE, measured in operando using a FaS-PhoReS. Previous research on TiO_2-coated planar silica substrates demonstrated that the design of FaS-PhoReS ensures that the results are independent of (i) evaporation of the aqueous dye solution and also (ii) not strongly affected by environmental parameters such as temperature and humidity [37]. MO and T85 were chosen due to their demonstrated excellent stability under simulated sunlight in a previous work [37], which means that photolysis makes a negligible contribution to the total photodegradation observed. Figure 6a,b illustrates that the initial absorbance was about 0.50 for MO and 0.45 for T85, respectively, across the 2.0 cm dye solution in the well (corresponding to an optical absorption coefficient of 2.46×10^4 L·M^{-1}·cm^{-1} for MO [2, 59] and 2.1761×10^4 L M^{-1} cm^{-1} for T85) [60]. A significant decrease in the absorption spectra of MO (Figure 6a) and T85 (Figure 6b) over time occurs due to the ROS generated by the TiO_2-coated (700 cycles, FA at 600°C) QFF-based PCMs. After 360 min of light exposure, both dyes have been significantly photodegraded, and the level of absorbance remaining is in the range of about 0.05 (MO)–0.02 (T85). In comparison, it can be seen that only a slight reduction in dye absorbance (0.35 for MO and 0.4 for T85) is observed over

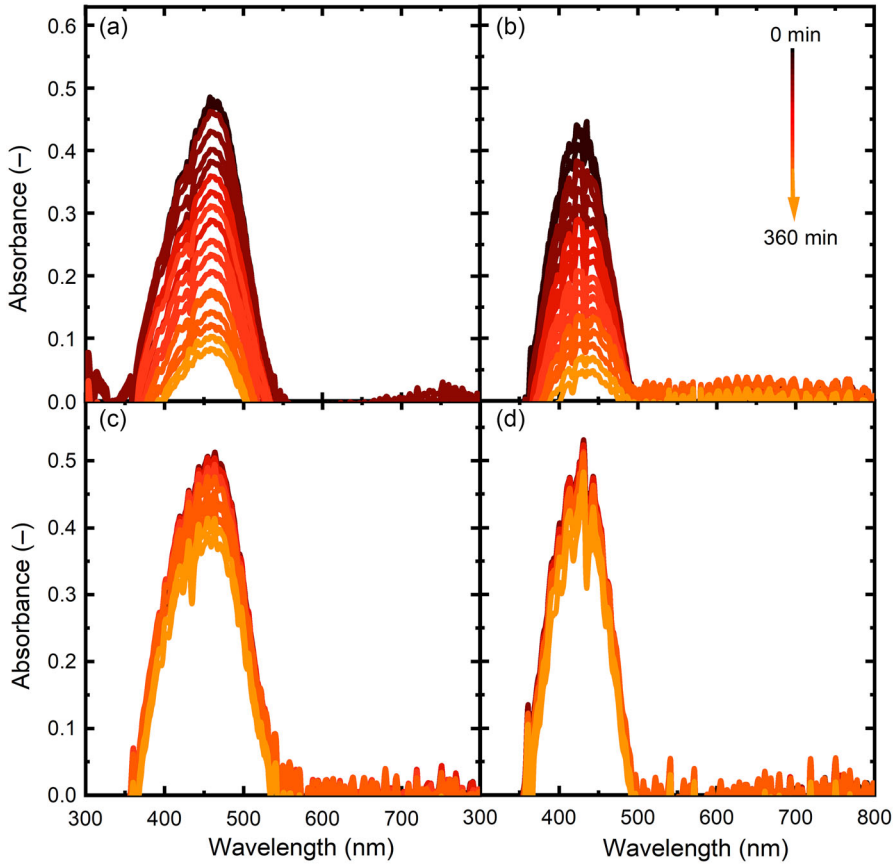

FIGURE 6 | In operando photodegradation testing using FaS-PhoReS, showing the time evolution (0–360 min) absorption spectra of 20 mL of two dyes at a 0.01 mM concentration—(a) MO and (b) T85—using a TiO_2-coated (700 cycles, FA at 600°C) QFF PCM. The same testing is then conducted using a TiO_2-coated (700 cycles, RTA at 500°C) PTFE-based PCM on the same two dyes: (c) MO and (d) T85.

the same timeframe when using the annealed TiO_2 (700 cycles, RTA at 500°C)-coated PTFE-based PCMs, as shown in Figure 6c,d. This is symptomatic of the limited thickness and poorer crystallinity of the TiO_2 films on the PTFE-based PCM. Additionally, Figure S23 presents the temporal variation of absorption spectra of MO and T85 dye solution due to 700 cycles of TiO_2 films coated onto the planar silica.

3.5 | TiO_2 PCMs: Removal is a Function of Film Thickness

To evaluate whether the photocatalytic degradation might be limited by film thicknesses, and specifically by the limited diffusion length of charge carriers, FaS-PhoReS experiments similar to those described above were conducted using as-deposited TiO_2 coated onto the QFF-based PCMs. Figure 7a,b demonstrates that, first, the dyes were not removed by photolysis alone (a directional reaction of sunlight with the dye), indicating the photocatalysis was responsible for the removal. Second, the removal efficiency of both dyes steadily increased as a function of TiO_2 film thickness. For example, the removal efficiency of 45% for MO was measured for the thinnest films (300 cycles, 11.90 nm), increasing to 49%, 54%, 63%, and 66% as the film thickness increased to 15.60 nm (400 cycles), 20.30 nm (500 cycles), 23.87 nm (600 cycles), and 28.05 nm (700 cycles), respectively (see Figure 7a). The removal efficiency trend and values were very similar for T85 (Figure 7b), with values of 47%, 53%, 57%, 65%, and 68% being measured for the same range of sample thicknesses. The monotonic increase in the photodegradation efficiency as a function of thickness (11.90–28.05 nm) is due to an increase in UV maximum absorbance of 0.66, 0.74, 0.78, 0.8, to 0.85 (Figure S17). This suggests that the lower removal with thinner films is attributed to inefficient harvesting of photons, which then improves at greater thicknesses. Further, from the thickness range investigated here (11.9–28 nm), it is important to note that the performance is not limited by the diffusion lengths of the excited charge carriers, which manage to penetrate from the bulk to the surface of TiO_2 to drive the redox reaction [61]. In addition, Figure S24a,b illustrates the removal efficiency of MO and T85 dye solutions using TiO_2 films coated onto planar silica.

Furthermore, the turnover numbers of degraded dye molecules and apparent quantum yields (AQYs) as a function of film thickness (11.90–28 nm) were also assessed to evaluate the photocatalytic performance of the ultrathin TiO_2 films coated on the fused silica substrate (more details in Sections S12 and S13). The results show the turnover number of 0.33 for MO at a thickness of 11.90 nm, decreasing to 0.23 at 28.05 nm (Table S6). This trend is due to an increase in the number of degraded dye molecules as the film thickness grows. It suggests that the number of dye molecules adsorbed onto TiO_2 as a function of film thickness likely blocks the active sites. A similar pattern was observed for T85, with a turnover number of 0.34 at 11.90 nm, then declining to 0.24 at 28.05 nm. The low estimated turnover numbers are likely related to the ultrathin layer of TiO_2, which generates fewer active sites.

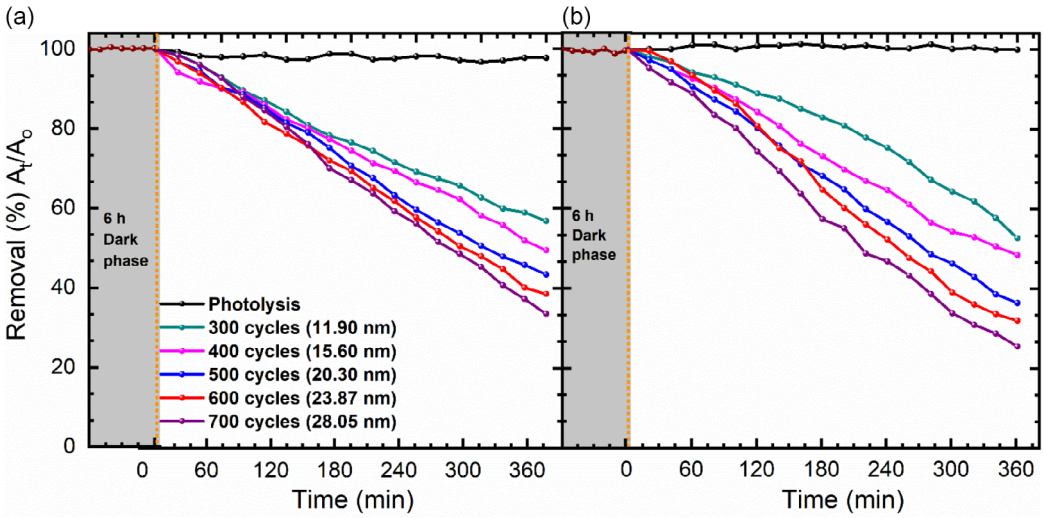

FIGURE 7 | In operando degree of removals as a function of film thickness of the as-deposited TiO_2 ultrathin films on QFF during the photocatalytic degradation of 20 mL of the 0.01 mM (a) MO and (b) T85 dye aqueous solution after 360 min. For completeness, the negligible removal occurring due to photolysis and in the dark with TiO_2 coated-QFF (600°C) is also plotted.

The estimated AQYs were found to increase from 4.71×10^{-7}% (11.90 nm) to 8.09×10^{-7}% (28.05 nm) during the photocatalytic degradation of MO (Table S8). The increase is attributed to an extension of the optical absorption as a function of TiO_2 film thickness. The lower AQY values are likely attributed to the ultrathin layer of TiO_2 films. A similar observation was also noted for degradation of T85 in which the AQY increased from 4.80×10^{-7}% to 8.48×10^{-7}%. The AQYs in this work, which are limited to the TiO_2 thin layers, were significantly lower than those calculated by Ralph Stephen [62] in the 6×10^{-3}–1.5×10^{-2} range in the degradation of phenol using P25 TiO_2 nanoparticles with a size of 30 nm, which obviously have a significantly larger specific surface area than thin films [63].

3.6 | TiO_2 PCMs: Removal Is a Function of Annealing Temperature

The results in Figure 8 summarize the removal efficiency of MO and T85 in the dark and presence of light due to direct photolysis, pristine QFF, PTFE, and as a function of temperatures with 700 cycles of ultra-TiO_2 thin films coated on the QFF and PTFE. The results exhibit almost no photodegradation efficiency with pristine QFF and PTFE. Figure 8a illustrates the photocatalytic degradation efficiency of about 66% of MO with as-deposited (250°C) TiO_2 film-coated QFF. An increase in the degree of removal to about 72% with annealing at 300°C is seen. The highest removals of 88%–94% were observed from 500°C to 700°C, remained stable, then declined for annealing above 900°C, and dropped to about 76% at 1000°C and 66% at 1100°C. The trend of the degree of photodegradation was also observed for T85 (Figure 8b) with values of 68%, 76%, 90%–96%, 78%, and 74% following the similar trends of temperatures as for MO. The minimal photodegradation at lower annealing temperatures is ascribed to the weak crystallinity phases, which are limited by the grain boundary defect states that act as detrimental sites for the photogenerated charge carriers [7, 64]. The higher removals with films annealed at 500°C, 700°C, and 900°C are ascribed to the increased optical absorption, attributed to the high degree of crystallinity of the anatase with a large active surface area of the crystallite that can absorb sufficient light energy [50]. The decline of performance at high annealing temperatures (>1000°C) is ascribed to the inactive surface area of TiO_2 crystals, which reduces the ability to absorb photons. Figures S25–S27, for other film thicknesses coated onto the QFF substrate, also exhibit a similar trend of photocatalytic degradation. The photographs in Figure S28 represent the well arrangement containing the dye solution and 2×2 cm of QFF coated with TiO_2 films before and after 360 min of light irradiation during the photocatalytic degradation.

Figure 8c demonstrates the removal efficiency of 12.5% (MO) with as-deposited (250°C) 700 cycles TiO_2 films-coated PTFE and from 13% to 33% when annealed (300°C–500°C) at RTA. The performance was increased up to 36% at an annealing temperature of 300°C in FA. A similar trend was observed for T85 (Figure 8d) with removals of 6%–9% in RTA and 18% in FA. The poorer performance is attributed to weaker absorption of photons, caused by the greatly reduced TiO_2 growth rates on the hydrophobic PTFE membrane (as explained in the XRD and EDX analysis above), thus lowering the photocatalytic activity. A similar trend is exhibited for other films (300, 400, 500, and 600 cycles) coated on/in the PTFE as presented in Figures S29 and S30, while Figure S31 photographs illustrate the photocatalytic performance of the TiO_2 films coated – PTFE, before and after photodegradation of the MO and T85 dye solution. Besides, Figures S32 and S33 display removal efficiencies with TiO_2 films (300, 400, 500, 600, and 700 cycles) coated on a planar silica substrate as the reference.

Furthermore, Table S7 presents the turnover numbers of MO and T85 dye molecules with a 700 cycle TiO_2 film as a function of annealing temperature. The findings reveal that the increase in MO turnover numbers from 0.27 (300°C) to 0.35 (700°C) is attributed to the increase in the degree of crystallinity of the TiO_2. The decline of turnovers up to 0.02 at 1100°C is ascribed to the change in surface roughness of active TiO_2 crystals at very high annealing temperatures. This is because larger crystals at elevated temperatures exhibit signs of grain coarsening, leading to reduced surface area [52]. A similar trend was observed for

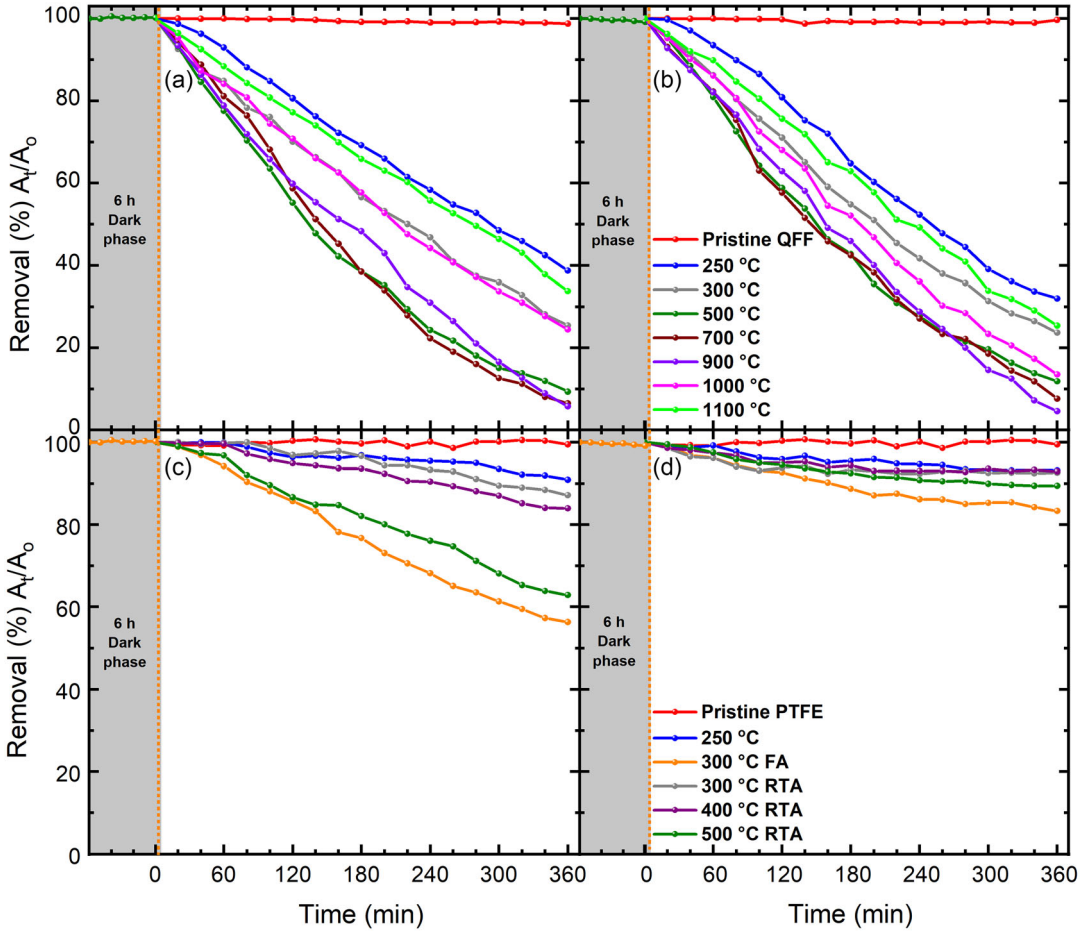

FIGURE 8 | In operando removal efficiency of 20 mL of 0.01 mM initial concentration of (a) MO and (b) T85 dye aqueous solution after 360 min in the dark and under the presence of light under direct photolysis, pristine QFF, and as-deposited (250°C) 700 cycles TiO_2 ultrathin films-coated QFF and annealed films in FA for 1 h in air, whereas removal efficiency in (c) MO and (d) T85 is due to pristine PTFE and as-deposited (250°C) 700 cycles TiO_2 ultrathin films-coated PTFE and annealed at 300°C in FA and RTA from 300 to 500°C for 3 min.

T85, with turnovers increasing from 0.27 at 300°C to 0.35 at 700°C and then dropping to 0.02 at 1100°C. In addition, the estimated TiO_2 molecules of the annealed films (Table S7) are slightly lower than those of the as-deposited TiO_2 films (Table S6) due to a decrease in the thickness of the annealed films, which is attributed to the densification of the thin film and decrease in the concentration of chlorine and hydrogen impurities from the $TiCl_4$ precursor and the water oxidant, respectively, which often decline at elevated temperatures [46, 47].

Moreover, the increase in AQYs (Table S9) from 9.64×10^{-7}% to 1.20×10^{-6}% in the degradation of MO with annealed (300°C–700°C) 700 cycles TiO_2 is attributed to film crystallinity, which increases the lifetime of charge carriers to generate sufficient ROSs. The decline of the AQY at 900°C from 2.19×10^{-7}% to 5.97×10^{-8}% at 1100°C is ascribed to the inactive specific surface area of the TiO_2 crystals at elevated temperatures [65, 66]. The trend was also observed for T85, in which the AQY increased from 9.58×10^{-7} to 1.25×10^{-6}% and then dropped to 5.73×10^{-8}% at 1100°C. The calculated values are low compared to the study of Emeline et al. [67], which reported AQY of 5.7×10^{-3}% during the photodegradation of phenol with P25 TiO_2 nanoparticles with size of 30 nm. The study by Yan et al. [43] reported significant AQYs of 0.2% and 0.3% with sulfur-doped titania (S–TiO_2) and P25 TiO_2 nanoparticles on MB degradation. On the other hand, the author also reported a minimal AQY of 5×10^{-5}% under visible light, attributed to the low absorbance of the diluted MB solutions. The great difference between our estimated AQY values and those reported in the literature is likely due to the thin layer of TiO_2 materials and the low diffusion rate of adsorption–desorption equilibrium on the surface of the photocatalysts [68].

3.7 | TiO_2 PCMs: Performance of Nonstoichiometric TiO_{2-x} Films

Previously, the optical absorption of oxygen-deficient A-TiO_{2-x} (700 cycles, FA at 500°C in forming gas) ultrathin films coated on QFF substrate was shown to be significantly higher than that of pure anatase (700 cycles, FA at 500°C in air for 1 h) films. In this section, the photocatalytic performance of both of these QFF-based PCMs is compared using the photodegradation of MO and T85 dye aqueous solutions. The results in Figure 9a,b demonstrate that the degree of photodegradation due to a TiO_{2-x}, coated PCM (red curve) indeed outperforms that of the TiO_2 -coated PCM (magenta curve) by about 98% (MO) and 100% (T85), respectively, both under the MH full spectrum. The MH lamp used in FaS-PhoReS has a relatively rich UV spectrum [37], which then begs the question: how do the TiO_{2-x}

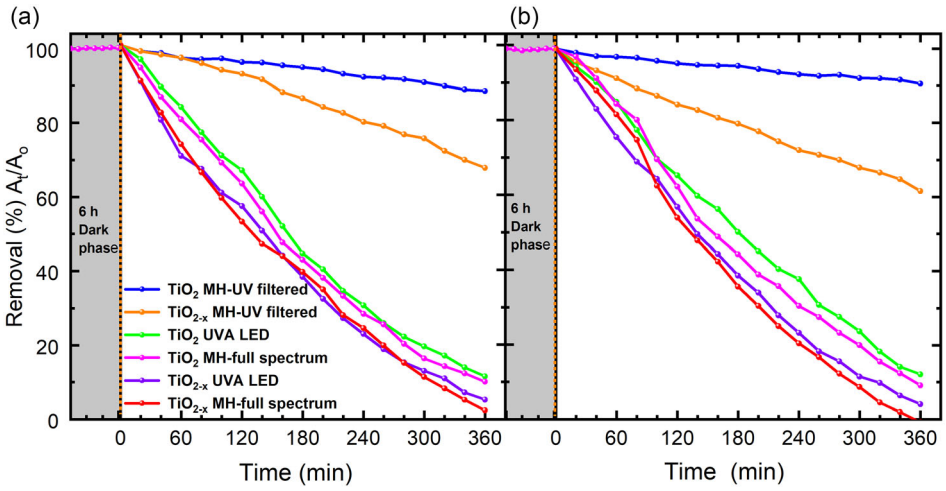

FIGURE 9 | The comparison of the degree of photodegradation of 20 mL of 0.01 mM initial concentration of (a) MO and (b) T85 dye solution after 360 min in the dark, with solar simulator MH lamp (full spectrum and UV filtered) and UVA-LED using the annealed (500°C in air for 1 h) pure ultrathin TiO_2 films and TiO_{2-x} treated at 500°C for 1 h in flow of H_2 (4%)/Ar (96%), both coated on QFF.

samples perform under a solar spectrum that contains no UV? To answer this, a 10 mm-thick polycarbonate sheet was placed between the solar simulator and the sample trays of FaSPhoReS. This effectively removed all UV below 400 nm from the spectrum, plus also reduced the overall intensity by 8% (see Figures 2 and S36) due to increased reflectance losses in the system. From Figure 9, it can be seen that the performance of the TiO_{2-x}-coated PCM under the MH-UV filtered spectrum results revealed low removal (32% MO and 38% T85 removals, yellow curves); however, it is significant that this contribution comes from visible light alone. In contrast, the pure TiO_2-coated PCM achieved removal efficiencies of 12% for MO and 10% for T85 (blue curves) under the same filtered illumination. The increased removal of TiO_{2-x} films compared to pure TiO_2, in the visible range, is attributed to interband energy levels of oxygen vacancies, which narrows the bandgap [17, 69]. In addition, the oxygen vacancy improves charge carrier separation and increases the diffusion length from the bulk into the surface of TiO_{2-x} to participate in the production of superoxide ions and hydroxyl radicals, which potentially degrade the dye molecules [57]. Interestingly, the TiO_{2-x} showed (Table S7) higher turnover numbers of 0.37 (MO) and 0.38 (T85), compared to 0.33 (MO) and 0.34 (T85) for the stoichiometric A-TiO_2. The higher turnover due to TiO_{2-x} is attributed to the presence of the oxygen vacancies, which boost the photocatalytic performance.

Furthermore, to test for possible photosensitization effects of MO and T85 dye on the PCMs, an experiment using UVA-LED (365 nm) illumination was performed, which was then compared to MH-UV filtered (visible light, $\lambda > 400$ nm) as well as the MH-full spectrum of simulated sunlight. As shown in Figure 8a for TiO_2, the MO removal is 91% under UVA-LED (green curve) compared to 12% with MH-UV filtered (blue curve), and the latter is eight times lower than the removal with MH-full spectrum. A similar pattern appears when using the T85 dye (Figure 8b), where 88% removal was achieved under UVA-LED illumination and 10% with the MH-UV filtered lamp, while 100% removal occurred with the MH-full spectrum. The 10%–12% removal efficiencies of the dyes under visible illumination are attributed to dye photosensitization of the TiO_2. It should be noted that this removal is very limited compared to the much higher performance of the TiO_2 PCM under both UV light and MH-full spectrum, indicating that the efficiencies are indeed mainly dominated by TiO_2 bandgap photoexcitation, rather than MO and T85 photosensitization. For the TiO_{2-x} PCMs, the level of removal efficiency under the MH-UV filtered illumination was significantly higher at 32% and 38% for MO and T85 illumination, as shown by the yellow curves in Figure 8a,b, respectively. The removal of both dyes via TiO_{2-x} under UVA-LED illumination remained high, the removals were 95%–97% (violet curves in Figure 8a,b), while near-100% removal was achieved under MH-full spectrum illumination (red curves in Figure 8a,b). Future work experiments will aim to resolve whether the increased dye removal under visible illumination is predominantly caused by dye sensitization, as in the case of TiO_2 above, or color centers in the TiO_{2-x} via action spectral [70] and anerobic reductive photocatalysis [71].

The findings also highlight an AQY of about 1.29×10^{-6}% for MO (Table S9) with TiO_{2-x} under MH-full spectrum, slightly higher than 1.27×10^{-6}% with UVA-LED and double that under MH-UV filtered light (8.34×10^{-7}%). The higher AQYs are attributed to the fraction of UV-energetic photons in the MH-full spectrum and UVA-LED that induce energetic charge carriers compared to less energetic photons under MH-UV filtered. A similar trend was also noted for T85, in which the AQYs of about 1.30×10^{-6}%, 1.28×10^{-6}%, and 8.94×10^{-7}% were estimated under MH-full spectrum, UVA-LED, and MH-UV filtered, respectively. The obtained values differ from those of the study of Ali and Kim [72], which reported the AQYs in the 3.22–9.11×10^{-5}% range during the degradation of methylene blue with TiO_2 nanotubes and reduced graphene TiO_2 nanotubes. The difference is likely attributed to the ultrathin layer of our TiO_2 samples and possibly due to the low rate of activation of dye molecules into the active surface and deactivation of final products from the surface of TiO_2 [68]. Furthermore, Figure S34 presents removal efficiencies with 700 cycles TiO_{2-x} film-coated silica as the reference.

3.8 | TiO_2 PCMs: Photocatalytic Reaction Kinetics

Building on the results of the previous section, the same two PCMs, 700 cycle TiO_2 (250°C–1100°C, and TiO_{2-x} ultrathin films coated on QFF, were chosen to study the photocatalytic kinetics. To quantify the photocatalytic activity, the Langmuir–Hinshelwood kinetic model was employed to estimate the photocatalytic degradation rate constant [73]. The linear fitting of Equation (2)

$$\ln\left(\frac{A_t}{A_o}\right) = -k_{app}t \quad (2)$$

to experimental data was employed to determine the pseudo apparent rate constant (k_{app} min^{-1}), where A_o is an initial dye absorbance before irradiation, A_t is the absorbance as a function of irradiation time, and t is the residence time. The values of k_{app} were determined from the slope via the linear fitting of the regression coefficient (R^2), ranging from 0 to 1. The higher value of the correlation coefficient R^2 close to 1 describes the best fit to the experimental data, and the higher value of k_{app} indicates the better photocatalytic activity.

Figure 10 illustrates the linear relationship of $\ln(A_t/A_o)$ against irradiation time, and Table 3 displays the values of R^2 and k_{app} during the photodegradation of MO and T85 dye solution in the absence and presence of the TiO_2 ultrathin films. The findings revealed the values of R^2 in the range of 0.97–0.99, which reflects a very good fitting of the experimental data, except during the photolysis, which revealed a value of 0.74. These values indicate that the photocatalytic degradation of MO and T85 dyes follows pseudo-first-order kinetics. The results reveal the lowest k_{app} of 1.78×10^{-6} min^{-1} for MO and 1.72×10^{-6} min^{-1} for T85 during the photolysis.

In contrast, Figure 10a revealed a lower k_{app} of 0.0026 min^{-1} for as-deposited TiO_2 films and a higher value of 0.0062 min^{-1} for annealed at 500°C due to degradation of MO. At a higher annealing temperature of 1100°C, the rate dropped to 0.0036 min^{-1}. Interestingly, the TiO_2 films exhibited the highest k_{app} of 0.0073 min^{-1}. Figure 10b for T85 follows a similar trend with a lower rate of 0.0025 min^{-1} with as-deposited films and 0.0058 min^{-1} of annealed (500°C) and dropped to 0.0031 min^{-1} at 1100°C, while 0.0075 min^{-1} was achieved with TiO_{2-x}. The findings signify that TiO_{2-x} performed better than the

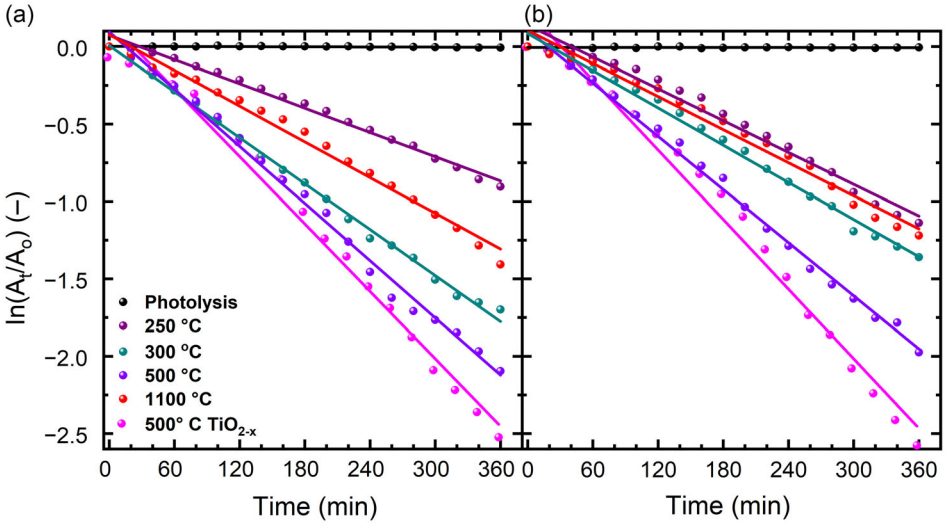

FIGURE 10 | The L–H photodegradation kinetics due to 700 cycles TiO_2 (250°C–1100°C) and TiO_{2-x} films-coated QFF on 20 mL of 0.01 mM initial concentration of (a) MO and (b) T85 dye aqueous solution after 360 min of light irradiation.

TABLE 3 | Pseudo-first-order kinetic photocatalytic constants (k_{app}) and linear regression coefficients (R^2) for photocatalytic degradation of MO and T85 dye aqueous solutions using TiO_2-coated QFF membranes annealed in either (i) air (TiO_2) at 300, 500, and 1100°C or (ii) forming gas at 500°C (TiO_{2-x}).

Sample	Model pollutant	Parameters	Photolysis	250°C	300°C	500°C	1100°C
TiO_2 coated QFF	MO	k_{app} (min^{-1})	1.78×10^{-6}	0.0026	0.0049	0.0062	0.0036
		R^2	0.74	0.99	0.99	0.99	0.97
	T85	k_{app} (min^{-1})	1.72×10^{-6}	0.0025	0.0038	0.0058	0.0031
		R^2	0.76	0.97	0.98	0.99	0.99
TiO_{2-x} coated QFF	MO	k_{app} (min^{-1})	1.78×10^{-6}	—	—	0.0073	—
		R^2	0.74	—	—	0.99	—
	T85	k_{app} (min^{-1})	1.72×10^{-6}	—	—	0.0075	—
		R^2	0.76	—	—	0.98	—

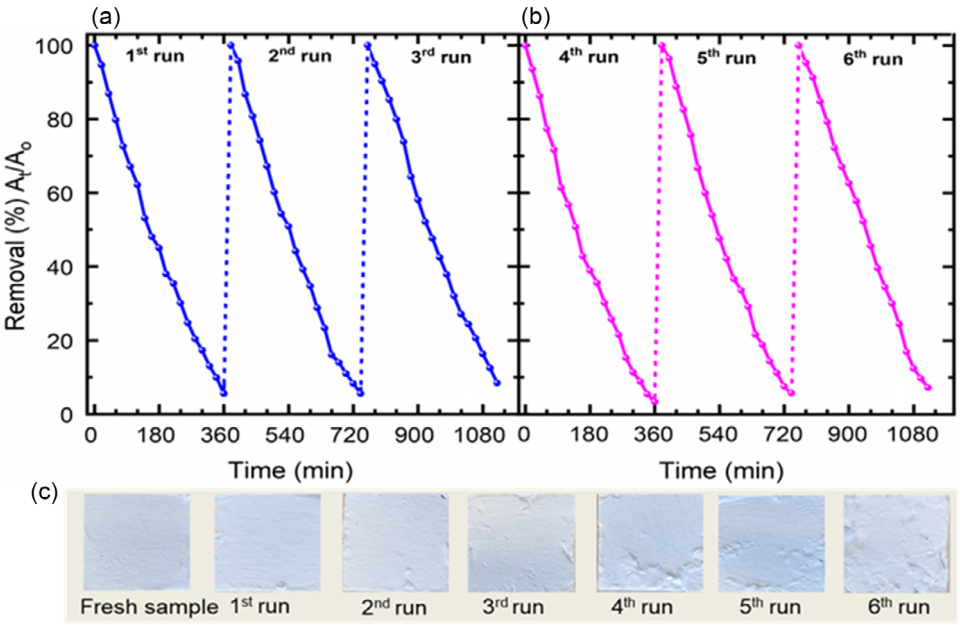

FIGURE 11 | The photodegradation performance of 700 cycles TiO_2 ultrathin films-coated QFF annealed at 600°C for 1 h in air for the degradation of 20 mL of 0.01 mM (a) MO and (b) T85 during six consecutive reaction cycles, whereas (c) represents the images of the QFF coated with TiO_2 fresh sample before the 1st run and then after each run (1–6).

stoichiometric TiO_2 films. Additionally, Figure S35 illustrates the photocatalytic kinetics for other annealing temperatures, and Table S5 highlights their linear correlation coefficients and degradation rate constants.

3.9 | TiO_2 PCMs: Robustness

To check the robustness of the TiO_2-coated membranes over multiple photodegradation cycles, the photocatalytic removal and stability of TiO_2 (700 cycles, 600°C)-coated QFF-based PCMs were tested for a total of six runs: three for degrading MO and the other three for T85, as illustrated in Figure 11. The TiO_2 films coated on QFF were chosen because they exhibited the best photocatalytic performance. For these test experiments, 20 mL of 0.01 mM MO was dispersed into the wells containing the TiO_2 films for the 1st run for 360 min. Subsequently, the 2nd and 3rd runs of MO were conducted after the films were washed with DI water. After MO runs were completed, the films were rinsed with DI water five times to ensure no MO dye molecules were contaminated and then stored at room temperature for 12 h before T85 runs. Then, T85 degradation experiments were carried out for three consecutive runs in a similar manner.

Figure 11a,b presents the degree of photodegradation of MO and T85 after three simultaneous runs for each. Figure 11c depicts the images of the QFF coated with TiO_2 ultrathin film surface morphology appearance before and after the 1st, 2nd, and 3rd successive runs for MO and the 4th, 5th, and 6th runs for T85. The results reveal removal efficiencies of 96%, 95%, and 93% for the 1st, 2nd, and 3rd repeats of MO, respectively, with minimal deviation. For T85, efficiencies of 94%, 91%, and 89% were observed for the 4th, 5th, and 6th runs, respectively. The decrease in efficiency is likely due to delamination of QFF throughout the cycling tests. This is evident with QFF surface morphology appearance as indicated in Figure 11c, where slight damage to the structure starts appearing within the first three repeats. This then worsens during the 4th to the 6th repeats, where the QFF membrane begins to swell and/or the TiO_2 film starts to delaminate due to prolonged interaction time with the dye solution, thus slightly reducing its performance. The results reveal the reusability of the films with relatively high retention of performance. Thus, the TiO_2 ultrathin films on QFF are fairly stable for long-term applications with a very slight decrease in degradation efficiency.

4 | Conclusion

In this study, the as-deposited (250°C) ALD TiO_2 ultrathin films-coated QFF demonstrated an increase in XRD peak intensity as a function of thickness (300 cycles /11.90 nm to 700 cycles /28.05 nm), while no peaks were observed for films on the PTFE membrane. The annealed TiO_2 films-coated QFF revealed a significant increase in peak intensity with FA and a slight increment with RTA (300°C–500°C). At elevated annealing temperatures from 600°C to 1100°C, TiO_2 films-coated QFF did not exhibit A–R mixed phases, except the films grown on silicon wafers, which displayed mixed phase above 400 cycles at annealing temperatures beyond 800°C. The annealed TiO_2 films coated on PTFE exhibited weak anatase peak intensity for 700 cycles, and below it, no peaks were observed. The SEM images confirmed the presence of TiO_2 coated on the membrane fibers, while the EDX profile revealed that the TiO_2 film deposited onto QFF is about three times greater than on PTFE. The high UV absorption below 395 nm was achieved with TiO_2 films coated on QFF compared to films on PTFE, which absorbs below 360 nm. The TiO_{2-x} films extended light absorption to the vis–NIR region. The bandgaps of 3.2 and 3.4 eV were achieved with TiO_2 films coated on QFF and PTFE, respectively, whilst the value of 3.10 eV was achieved for TiO_{2-x} films. In photocatalytic testing, it was found that the removal efficiency of MO is linear

with increasing film thickness from 47% (11.9 nm) to 67% (28.05 nm). A similar trend was observed for T85 from 49% to 65%. The annealed TiO_2 films coated on QFF exhibited an increase in removal efficiency to about 80%–97% as a function of temperature range up to 900°C and dropped to about 76% and 66% at annealing temperatures of 1000°C and 1100°C, respectively. The TiO_2 films coated on PTFE demonstrated very minimal performance. The best performance was achieved with TiO_{2-x} films, which showed efficiencies of up to 98% for MO and 100% for T85. Photocatalytic performance under MH-UV filtered showed negligible removals compared to UVA and MH-full spectrum.

Author Contributions

Elisante M. Maloda: conceptualization (supporting), data curation (lead), formal analysis (lead), investigation (lead), methodology (supporting), validation (lead), visualization (lead), writing – original draft (lead). **Justine S. Nyarige**: conceptualization (supporting), data curation (supporting), formal analysis (supporting), investigation (supporting), methodology (supporting), supervision (supporting), visualization (supporting), writing – review & editing (supporting). **Dmitry Busko**: software (supporting), validation (supporting). **Andrey Turshatov**: investigation (supporting), resources (supporting), validation (supporting). **Bryce S. Richards**: conceptualization (lead), formal analysis (supporting), funding acquisition (lead), methodology (equal), project administration (lead), resources (lead), supervision (lead), validation (supporting), visualization (supporting), writing – review & editing (lead)

Acknowledgments

The authors gratefully acknowledge financial support from the following sources: (i) the World Bank collaboration with the Dar es Salaam University College of Education via Higher Education for Economic Transformation (HEET) Project for providing a PhD scholarship to E.M.M. and ii) the Helmholtz Association – Research Field Energy – Materials and Technologies for the Energy Transition program (Topic 1 Photovoltaics and Wind Energy, 38.01.05).

Open Access funding enabled and organized by Projekt DEAL.

Funding

This study was supported by Helmholtz-Gemeinschaft (MTET Topic 1 (38.01.05)) and World Bank Group (PhD scholarship).

Conflicts of Interest

The authors declare no conflict of interest.

Data Availability Statement

The data that support the findings of this study are available from the corresponding author upon reasonable request.

References

1. J. De Decker, M. Verschueren, and B. Ávila "Published in 2017 by the United Nations Educational, Scientific and Cultural Organization, 7, place de Fontenoy, 75352 Paris 07 SP, France," (2017).

2. N. Pakharuddin, M. Fazly, S. A. Sukari, K. Tho, and W. Zamri, "Water Treatment Process Using Conventional and Advanced Methods: A Comparative Study of Malaysia and Selected Countries," presented at IOP Conference Series: Earth and Environmental Science, 2021.

3. A. I. Schäfer, I. Akanyeti, A. J. Semião, "Micropollutant Sorption to Membrane Polymers: A Review of Mechanisms for Estrogens," *Advances in Colloid and Interface Science* 164 (2011): 100.

4. A. Fujishima, X. Zhang, and D. A. Tryk, "TiO_2 Photocatalysis and Related Surface Phenomena," *Surface Science Reports* 63 (2008): 515.

5. A. Hagfeldt and M. Gratzel, "Light-induced Redox Reactions in Nanocrystalline Systems," *Chemical reviews* 95 (1995): 49-68.

6. M. Bekbölet, M. Lindner, D. Weichgrebe, and D. Bahnemann, "Photocatalytic Detoxification with the Thin-Film Fixed-Bed Reactor (TFFBR): Clean-up of Highly Polluted Landfill Effluents Using a Novel TiO2-Photocatalyst," *Solar Energy* 56 (1996): 455.

7. A. Fujishima, T. N. Rao, and D. A. Tryk, "Titanium Dioxide Photocatalysis," *Journal of Photochemistry and Photobiology C: Photochemistry Reviews* 1 (2000): 1.

8. M. Kapilashrami, Y. Zhang, Y.-S. Liu, A. Hagfeldt, and J. Guo, "Probing the Optical Property and Electronic Structure of TiO $_2$ Nanomaterials for Renewable Energy Applications," *Chemical Reviews* 114 (2014): 9662.

9. W. Fu, G. Li, Y. Wang, et al., "Facile Formation of Mesoporous Structured Mixed-Phase (Anatase/Rutile) TiO_2 with Enhanced Visible Light Photocatalytic Activity," *Chemical Communications* 54 (2018): 58.

10. J.-M. Herrmann, "Heterogeneous Photocatalysis: Fundamentals and Applications to the Removal of Various Types of Aqueous Pollutants," *Catalysis Today* 53 (1999): 115.

11. J. A. Rengifo-Herrera and C. Pulgarin, "Why Five Decades of Massive Research on Heterogeneous Photocatalysis, Especially on TiO2, Has Not yet Driven to Water Disinfection and Detoxification Applications? Critical Review of Drawbacks and Challenges," *Chemical Engineering Journal* 477 (2023): 146875.

12. M. R. Hoffmann, S. T. Martin, W. Choi, and D. W. Bahnemann, "Environmental Applications of Semiconductor Photocatalysis," *Chemical Reviews* 95 (1995): 69.

13. S. Ullah, E. P. Ferreira-Neto, A. A. Khan, I. P. Medeiros, and H. Wender, "Supported Nanostructured Photocatalysts: the Role of Support-Photocatalyst Interactions," *Photochemical & Photobiological Sciences* 22 (2023): 219.

14. G. Žerjav, K. Žižek, J. Zavašnik, and A. Pintar, "Brookite vs. Rutile vs. Anatase: What`s behind Their Various Photocatalytic Activities?," *Journal of Environmental Chemical Engineering* 10 (2022): 107722.

15. M. E. Aguirre, R. Zhou, A. J. Eugene, M. I. Guzman, and M. A. Grela, "Cu_2O/TiO_2 Heterostructures for CO_2 Reduction through a Direct Z-Scheme: Protecting Cu2O from Photocorrosion," *Applied Catalysis B: Environmental* 217 (2017): 485.

16. K. Murakoshi, G. Kano, Y. Wada, et al., "Importance of Binding States between Photosensitizing Molecules and the TiO2 Surface for Efficiency in a Dye-Sensitized Solar Cell," *Journal of Electroanalytical Chemistry* 396 (1995): 27.

17. R. Ratshiedana, M. E. Malefane, O. J. Fakayode, G. K. More, A. K. Mishra, and A. T. Kuvarega, "Ag Induced Plasmonic TiO2 for Photocatalytic Degradation of Pharmaceutical under Visible Light: Insights into Mechanism, Antimicrobial and Cytotoxicity Studies," *Materials Today Communications* 41 (2024): 110753.

18. A. L. Linsebigler, G. Lu, and J. T. Yates Jr, "Photocatalysis on TiO_2 Surfaces: Principles, Mechanisms, and Selected Results," *Chemical Reviews* 95 (1995): 735.

19. S. G. Ullattil, S. B. Narendranath, S. C. Pillai, and P. Periyat, "Black TiO_2 Nanomaterials: A Review of Recent Advances," *Chemical Engineering Journal* 343 (2018): 708.

20. J. Hu, S. Zhang, Y. Cao, H. Wang, H. Yu, and F. Peng, "Novel Highly Active Anatase/Rutile TiO_2 Photocatalyst with Hydrogenated Heterophase Interface Structures for Photoelectrochemical Water Splitting into Hydrogen," *ACS Sustainable Chemistry & Engineering* 6 (2018): 10823.

21. P. Deák, B. Aradi, and T. Frauenheim, "Band Lineup and Charge Carrier Separation in Mixed Rutile-Anatase Systems," *Journal of Physical Chemistry C* 115 (2011): 3443.

22. Z. Luo, A. S. Poyraz, C.-H. Kuo, et al., "Crystalline Mixed Phase (Anatase/Rutile) Mesoporous Titanium Dioxides for Visible Light Photocatalytic Activity," *Chemistry of Materials* 27 (2015): 6.

23. R. V. Nair, V. S. Gummaluri, M. V. Matham, and C. Vijayan, "A Review on Optical Bandgap Engineering in TiO_2 Nanostructures via Doping and Intrinsic Vacancy Modulation towards Visible Light Applications," *Journal of Physics D: Applied Physics* 55 (2022): 313003.

24. S. Chen, Y. Xiao, Y. Wang, Z. Hu, H. Zhao, and W. Xie, "A Facile Approach to Prepare Black TiO_2 with Oxygen Vacancy for Enhancing Photocatalytic Activity," *Nanomaterials* 8 (2018): 245.

25. M. Hatat-Fraile, R. Liang, M. J. Arlos, et al., "Concurrent Photocatalytic and Filtration Processes Using Doped TiO2 Coated Quartz Fiber Membranes in a Photocatalytic Membrane Reactor," *Chemical Engineering Journal* 330 (2017): 531.

26. C. S. Raota, S. Lotfi, R. Lyubimenko, B. S. Richards, and A. I. Schäfer, "Accelerated Ageing Method for the Determination of Photostability of Polymer-Based Photocatalytic Membranes," *Journal of Membrane Science* 686 (2023): 121944.

27. T. E. Berger, C. Regmi, A. I. Schäfer, and B. S. Richards, "Photocatalytic Degradation of Organic Dye via Atomic Layer Deposited TiO_2 on Ceramic Membranes in Single-Pass Flow-Through Operation," *Journal of Membrane Science* 604 (2020): 118015.

28. R. Lyubimenko, A. Turshatov, A. Welle, P. G. Weidler, B. S. Richards, and A. I. Schäfer, "Enhanced Photocatalytic Efficiency via Improved Contact in a Solar-Driven Membrane Reactor for Steroid Hormone Removal," *Chemical Engineering Journal* 451 (2023): 138449.

29. A. Y. Shan, T. I. M. Ghazi, and S. A. Rashid, "Immobilisation of Titanium Dioxide onto Supporting Materials in Heterogeneous Photocatalysis: A Review," *Applied Catalysis A: General* 389 (2010): 1.

30. T. J. Knisley, L. C. Kalutarage, and C. H. Winter, "Precursors and Chemistry for the Atomic Layer Deposition of Metallic First Row Transition Metal Films," *Coordination Chemistry Reviews* 257 (2013): 3222.

31. J. Hämäläinen, M. Ritala, and M. Leskelä, "Atomic Layer Deposition of Noble Metals and Their Oxides," *Chemistry of Materials* 26 (2014): 786.

32. K. J. Kumar, N. R. C. Raju, and A. Subrahmanyam, "Thickness Dependent Physical and Photocatalytic Properties of ITO Thin Films Prepared by Reactive DC Magnetron Sputtering," *Applied Surface Science* 257 (2011): 3075.

33. T. Luttrell, S. Halpegamage, J. Tao, A. Kramer, E. Sutter, and M. Batzill, "Why is Anatase a Better Photocatalyst than Rutile? - Model Studies on Epitaxial TiO_2 Films," *Scientific Reports* 4 (2014): 4043.

34. I. Levchuk, C. Guillard, F. Dappozze, S. Parola, D. Leonard, and M. Sillanpää, "Photocatalytic Activity of TiO_2 Films Immobilized on Aluminum Foam by Atomic Layer Deposition Technique," *Journal of Photochemistry and Photobiology A: Chemistry* 328 (2016): 16.

35. S. Vilhunen, M. Bosund, M.-L. Kääriäinen, D. Cameron, and M. Sillanpää, "Atomic Layer Deposited TiO_2 Films in Photodegradation of Aqueous Salicylic Acid," *Separation and Purification Technology* 66 (2009): 130.

36. S. Lotfi, K. Fischer, A. Schulze, and A. I. Schäfer, "Photocatalytic Degradation of Steroid Hormone Micropollutants by TiO_2-Coated Polyethersulfone Membranes in a Continuous Flow-through Process," *Nature Nanotechnology* 17 (2022): 417.

37. E. M. Maloda, L. S. Daniel, D. Busko, A. Turshatov, J. S. Nyarige, and B. S. Richards, "High-Throughput Photocatalytic Reactor With in Operando Characterisation for Fast Screening of Materials for the Photodegradation of Water-Borne Pollutants," *Advanced Materials Interfaces* 12 (2025): 2401000.

38. R.-S. Juang, C.-T. Hsieh, P.-A. Chen, and Y.-F. Chen, "Microwave-Assisted Synthesis of Titania Coating onto Polymeric Separators for Improved Lithium-Ion Battery Performance," *Journal of Power Sources* 286 (2015): 526.

39. K. Baba, S. Bulou, P. Choquet, and N. D. Boscher, "Photocatalytic Anatase TiO_2 Thin Films on Polymer Optical Fiber Using Atmospheric-Pressure Plasma," *ACS Applied Materials & Interfaces* 9 (2017): 13733.

40. J.-W. Jang and J.-W. Park, "Photocatalytic Performance of TiO_2 Films Produced with Combination of Oxygen-Plasma and Rapid Thermal Annealing," *Thin Solid Films* 520 (2011): 193.

41. H. Zhu, T. Pan, R. Sato, et al., "TiO_2/ p-Si Paste Heterojunction Fabricated by Rapid Thermal Annealing," *Applied Surface Science* 569 (2021): 151003.

42. M. Kao, H. Chen, and S. Young, "Dye-Sensitized Solar Cells with TiO2 Nanocrystalline Films Prepared by Conventional and Rapid Thermal Annealing Processes," *Thin Solid Films* 519 (2011): 3268.

43. X. Yan, T. Ohno, K. Nishijima, R. Abe, and B. Ohtani, "Is Methylene Blue an Appropriate Substrate for a Photocatalytic Activity Test? A Study with Visible-Light Responsive Titania," *Chemical Physics Letters* 429 (2006): 606.

44. M. Rochkind, S. Pasternak, and Y. Paz, "Using Dyes for Evaluating Photocatalytic Properties: A Critical Review," *Molecules* 20 (2014): 88.

45. A. S. f. Testing, M. C. G. o. Weathering, *Durability, Standard Tables for Reference Solar Spectral Irradiances: Direct Normal and Hemispherical on 37° Tilted Surface* (ASTM International, 2003).

46. I. Saric, R. Peter, I. K. Piltaver, I. J. Badovinac, K. Salamon, and M. Petravic, "Residual Chlorine in TiO_2 Films Grown at Low Temperatures by Plasma Enhanced Atomic Layer Deposition," *Thin Solid Films* 628 (2017): 142.

47. S. Kinnunen, J. Malm, K. Arstila, M. Lahtinen, and T. Sajavaara, "Characterization of ALD Grown TixAlyN and TixAlyC Thin Films," *Nuclear Instruments and Methods in Physics Research Section B: Beam Interactions with Materials and Atoms* 406 (2017): 152.

48. Q. Xu, Y. Yang, X. Wang, et al., "Atomic Layer Deposition of Alumina on Porous Polytetrafluoroethylene Membranes for Enhanced Hydrophilicity and Separation Performances, "*Journal of Membrane Science* 415 (2012): 435.

49. Y.-J. Shi, R.-J. Zhang, H. Zheng, et al., "Optical Constants and Band Gap Evolution with Phase Transition in Sub-20-nm-Thick TiO_2 Films Prepared by ALD,"*Nanoscale Research Letters* 12 (2017): 1.

50. I. J. Badovinac, R. Peter, A. Omerzu, et al., "Grain Size Effect on Photocatalytic Activity of TiO_2 Thin Films Grown by Atomic Layer Deposition," *Thin Solid Films* 709 (2020): 138215.

51. J. Banfield, "Thermodynamic Analysis of Phase Stability of Nanocrystalline Titania," *Journal of Materials Chemistry* 8 (1998): 2073.

52. H.-J. Koo, J. S. Jur, M. Woodroof, et al., "Stable Anatase TiO_2 Coating on Quartz Fibers by Atomic Layer Deposition for Photoactive Light-Scattering in Dye-Sensitized Solar Cells," *Nanoscale* 4 (2012): 4731.

53. P. Birnal, M. M. de Lucas, I. Pochard, B. Domenichini, and L. Imhoff, "Photocatalytic Properties of Atomic Layer Deposited TiO2 Inverse Opals and Planar Films for the Degradation of Dyes," *Applied Surface Science* 512 (2020): 145693.

54. M. Szindler, M. M. Szindler, P. Boryło, and T. Jung, "Structure and Optical Properties of TiO_2 Thin Films Deposited by ALD Method," *Open Physics* 15 (2017): 1067.

55. M. J. Arlos, M. M. Hatat-Fraile, R. Liang, et al., "Photocatalytic Decomposition of Organic Micropollutants Using Immobilized TiO2 Having Different Isoelectric Points," *Water Research* 101 (2016): 351.

56. R. G. Gordon, D. Hausmann, E. Kim, and J. Shepard, "A Kinetic Model for Step Coverage by Atomic Layer Deposition in Narrow Holes or Trenches," *Chemical Vapor Deposition* 9 (2003): 73.

57. B. Wang, H. Qi, Z. Liu, et al., "Structure, Chemical State and Photocatalytic Activity of TiO_{2-x} Nanostructured Thin Films by Glancing Angle Deposition Technique," *Journal of Alloys and Compounds* 716 (2017): 299.

58. N. Bazzanella, O. P. Bajpai, M. Fendrich, G. Guella, A. Miotello, and M. Orlandi, "Ciprofloxacin Degradation with a Defective TiO_{2-x} Nanomaterial under Sunlight," *MRS Communications* 13 (2023): 1252.

59. S. A. Daher, "Determining Values of Some Optical Constants for Some Colorants," *Journal of Education and Science* 25 (2012): 79–86.

60. G. Donoso, J. R. Dominguez, T. González, S. Correia, and E. M. Cuerda-Correa, "Electrochemical and Sonochemical Advanced Oxidation Processes Applied to Tartrazine Removal. Influence of Operational Conditions and Aqueous Matrix," *Environmental Research* 202 (2021): 111517.

61. K. Takanabe, "Photocatalytic Water Splitting: Quantitative Approaches toward Photocatalyst by Design," *ACS Catalysis* 7 (2017): 8006.

62. R. W. Matthews and S. R. McEvoy, "Photocatalytic Degradation of Phenol in the Presence of Near-UV Illuminated Titanium Dioxide," *Journal of Photochemistry and Photobiology A: Chemistry* 64 (1992): 231.

63. X. Chen and S. S. Mao, "Titanium Dioxide Nanomaterials: Synthesis, Properties, Modifications, and Applications," *Chemical Reviews* 107 (2007): 2891.

64. M. Schiavello, "Some Working Principles of Heterogeneous Photocatalysis by Semiconductors," *Electrochimica Acta* 38 (1993): 11.

65. L. Munguti and F. Dejene, "Influence of Annealing Temperature on Structural, Optical and Photocatalytic Properties of ZnO–TiO2 Composites for Application in Dye Removal in Water," *Nano-Structures & Nano-Objects* 24 (2020): 100594.

66. S. Bae, S. Kim, S. Lee, and W. Choi, "Dye Decolorization Test for the Activity Assessment of Visible Light Photocatalysts: Realities and Limitations," *Catalysis Today* 224 (2014): 21.

67. A. Emeline, A. Salinaro, and N. Serpone, "Spectral Dependence and Wavelength Selectivity in Heterogeneous Photocatalysis. I. Experimental Evidence from the Photocatalyzed Transformation of Phenols," *Journal of Physical Chemistry B* 104 (2000): 11202.

68. I. Groeneveld, M. Kanelli, F. Ariese, and M. R. van Bommel, "Parameters that Affect the Photodegradation of Dyes and Pigments in Solution and on Substrate – An Overview," *Dyes and Pigments* 210 (2023): 110999.

69. Q. Zhu, Y. Peng, L. Lin, et al., "Stable Blue TiO_{2-x} Nanoparticles for Efficient Visible Light Photocatalysts," *Journal of Materials Chemistry A* 2 (2014): 4429.

70. R. Quesada-Cabrera and I. P. Parkin, "Qualitative Approaches Towards Useful Photocatalytic Materials," *Frontiers in Chemistry* 8 (2020): 817.

71. S.-K. Lee, A. Mills, and N. Wells, "Assessing Photocatalytic Activity Using Methylene Blue without Dye Sensitisation," *Catalysis Today* 313 (2018): 211.

72. I. Ali and J.-O. Kim, "Continuous-Flow Photocatalytic Degradation of Organics Using Modified TiO_2 Nanocomposites," *Catalysts* 8 (2018): 43.

73. N. Barka, S. Qourzal, A. Assabbane, and Y. Ait-Ichou, "Kinetic Modeling of the Photocatalytic Degradation of Methyl Orange by Supported TiO_2," *Journal of Environmental Science and Engineering* 4 (2010): 1.

Supporting Information

Additional supporting information can be found online in the Supporting Information section. **Supporting Fig. S1**: Thickness and growth rate of as-deposited (250°C) TiO_2 films onto planar silica as a function of ALD cycles. **Supporting Fig. S2**: XRD patterns of the as-deposited (250°C) and annealed (300°C) 700 cycle TiO_2 films on pure PTFE. **Supporting Fig. S3**: XRD patterns of the as-deposited (250°C) TiO_2 films on (a) fused silica and (b) Si for 300, 400, 500, 600, and 700 cycles, compared with the ICSD reference of anatase TiO_2. **Supporting Fig. S4**: XRD patterns of the 700 cycles TiO_2 ultrathin films coated on (a) QFF and (b) Si, both annealed at FA from 600–1100°C. **Supporting Fig. S5**: XRD patterns of the as-deposited 600 cycles TiO_2-QFF and annealed at (a) RTA - (b) FA, TiO_2 -PTFE (c) RTA- (d) FA and TiO_2 -silica (e) RTA-(f) FA, along with ICSD reference patterns of anatase. **Supporting Fig. S6**: XRD patterns of the as-deposited 600 cycles TiO_2-Si and annealed in the FA, along with ICSD reference patterns of anatase and rutile TiO_2. **Supporting Fig. S7**: 500 cycles XRD patterns of as-grown TiO_2 film-coated QFF and annealed at (a) RTA - (b) FA, TiO_2 - PTFE (c) RTA-(d) FA, TiO_2 - silica (e) RTA-(f) FA along with ICSD reference of anatase. **Supporting Fig. S8**: 500 cycles XRD patterns of as-grown TiO_2 films-coated- Si annealed in the FA, along with the ICSD reference of anatase. **Supporting Fig. S9**: XRD patterns of the as-deposited 400 cycles TiO_2-coated QFF and annealed in the (a) RTA), (b) FA, both along with ICSD reference patterns of anatase. **Supporting Fig. S10**: XRD patterns of the as-deposited 400 cycles TiO_2 coated onto Si annealed in the FA, along with ICSD reference patterns of anatase. **Supporting Fig. S11**: 300 cycles XRD patterns of as-grown TiO_2 films coated on the QFF and annealed at (a) RTA - (b) FA, TiO_2 - PTFE (c) RTA-(d) FA, and TiO_2-coated silica (e) RTA-(f) FA, along with ICSD reference of anatase. **Supporting Fig. S12**: 300 cycles XRD patterns of as-grown TiO_2 films coated onto Si, annealed in FA, along with the ICSD reference of anatase. **Supporting Fig. S13**: 500 cycles XRD patterns of TiO_{2-x} thin films coated on the (a) QFF and (b) fused silica. **Supporting Fig. S14**: SEM surface morphologies of 700 cycles ALD TiO_2 thin films coated on PTFE annealed at 600°C RTA. **Supporting Fig. S15**: SEM surface morphologies of 700 cycles ALD TiO_2 ultrathin films coated on silica; (a) as-deposited and annealed at (b) 500°C and (c) 1100°C – both in FA. **Supporting Fig. S16**: (a) QFF fiber-coated TiO_2 films, while 3D AFM surface morphology images of 700 cycles TiO_2 films coated on QFF (b) as-deposited (250°C) and at annealing temperatures of (c) 500°C and (d) 1100°C in the FA. **Supporting Fig. S17**: UV-vis absorbance of the as-deposited and annealed (FA) TiO_2 ultrathin films coated on the QFF (a) 300 cycles, (b) 400 cycles, (c) 500 cycles, and (d) 600 cycles. **Supporting Fig. S18**: UV–vis absorbance of the as-deposited and annealed (RTA) TiO_2 ultrathin films coated on QFF (a) 300 cycles, (b) 400 cycles, (c) 500 cycles, and (d) 600 cycles. **Supporting Fig. S19**: UV–vis absorbance of the as-deposited and annealed TiO_2 ultrathin films coated on PTFE (a) 300 cycles, (b) 400 cycles, (c) 500 cycles, and (d) 600 cycles. **Supporting Fig. S20**: UV–vis absorbance of the 700 cycles TiO_2 ultrathin films coated on QFF annealed in (a) FA, (b) RTA, and (c) on PTFE in RTA. **Supporting Fig. S21**: Absorbance of the 700 cycles TiO_{2-x} ultrathin films compared to TiO_2, both coated on fused silica and annealed at 500°in forming gas. **Supporting Fig. S22**: Tauc plot bandgap of the as-deposited TiO_2 ultrathin films coated on (a) PTFE and (b) QFF, while (c) comparison of TiO_2 versus TiO_{2-x}, both annealed at 500°C. **Supporting Fig. S23**: Time evolution absorption spectra for uncoated silica on (a) MO and (b) T85, while (c) and (d) are respectively due to 700 cycles (28.05 nm) TiO_2 film-coated silica annealed at 600°C in the FA. **Supporting Fig. S24**: Influence of film thickness of TiO_2 films coated on planar silica as a reference on the photocatalytic degradation of 20 mL of the 0.01 mM (a) MO and (b) T85 dye solution after 360 min. **Supporting Fig. S25**: In operando removal efficiency of 20 mL of the 0.01 mM initial concentration of (a) MO and (b) T85 dye solution in dark (TiO_2 film annealed at 600°C) and presence of light under 700 cycles TiO_2 ultrathin films coated QFF annealed in the FA from 350 to 800°C in air for 1 h, while (c) MO and (d) T85 annealed in the RTA (300-500°C) for 3 min. **Supporting Fig. S26**: Removal efficiency of 20 mL of the 0.01 mM of (a) MO an (b)T85 dye solution after 360 min in dark (TiO_2 film annealed at 600°C) and presence of light with as- deposited (250°C) and annealed (300-1100°C in FA) 500 cycles TiO_2 coated-QFF, while (c) MO and (d) T85 with as- deposited (250°C) and annealed (300-1100°C in FA) 600 cycles TiO_2 coated-QFF- both after 360 min. **Supporting Fig. S27**: Degradation performance in dark (TiO_2 film annealed at 600°C) and presence of light with as-deposited (250°C) and annealed (300-1100°C in FA) 300 cycles TiO_2 films coated-QFF on degradation of 20 mL of the 0.01 mM (a)

MO and (b) T85, while as-deposited (250°C) and annealed (300-1100°C in FA) with 400 cycles (c) MO and (d) T85 – both after 360 min. **Supporting Fig. S28**: The photographs representing the well arrangement containing the dye solution and 2 x 2 cm of QFF coated with TiO_2 films for 500 cycles (1 to 15 well), and 700 cycles (16 to 30) to demonstrate the photocatalytic degradation of (a) MO, (b) T85 before light illumination and (c) MO, (d) T85 after 360 min of light irradiation. **Supporting Fig. S29**: The removal efficiency of 20 mL of the 0.01 mM (a) MO and (b) T85 dye solution after 360 min with as-deposited (250°C) and annealed (300°C in FA, 300-500°C in RTA) TiO_2 ultrathin films coated on PTFE for 300, while (c) MO and (d) T85 with 400 cycles annealed in FA at 300°C and RTA from 300-500°C. **Supporting Fig. S30**: Removal performance in dark (TiO_2 film annealed at 600°C) and presence of light with as-deposited (250°C) and annealed (300°C in FA, 300-500°C in RTA) 300 cycles TiO_2 films coated-PTFE on degradation of 20 mL of the 0.01 mM (a) MO and (b) T85, while as-deposited (250°C) and annealed (300°C in FA and 300-500°C in FA) 400 cycles on (c) MO and (d) T85 - both after 360 min. **Supporting Fig. S31**: The photographs (a, b) representing the well arrangement containing the dye solution and 2 x 2 cm of PTFE coated with TiO_2 films for 300 cycles (1 to 6), 400 cycles (7 to 12), 500 cycles (13 to 18), 600 cycles (19 to 24) and 700 cycles (24 to 30 well) to demonstrate the photocatalytic degradation of (a) MO, (b) T85 before light illumination while (c) MO, (d) T85 after 360 min of irradiation. **Supporting Fig. S32**: In operando removal efficiency of 20 mL of the 0.01 mM of (a) MO an (b)T85 dye solution in dark (TiO_2 film annealed at 600°C) and presence of light with as- deposited (250°C) and annealed (300-1100°C in FA) 300 cycles TiO_2 coated-silica, (c) MO and (d) T85 with as- deposited (250°C) and annealed (300-1100°C in FA) 400 cycles, while (e) MO and (f) T85 with as- deposited (250°C) and annealed (300-1100°C in FA) 500 cycles TiO_2 coated-silica- both after 360 min. **Supporting Fig. S33**: Degradation performance in dark (TiO_2 film annealed at 600°C) and presence of light with as-deposited (250°C) and annealed (300-1100°C in FA) 600 cycles TiO_2 films coated-silica on degradation of 20 mL of the 0.01 mM (a) MO and (b) T85, while (c) MO and (d) T85 with as- deposited (250°C) and annealed (300-1100°C in FA) 700 cycles TiO_2 coated-silica-both after 360 min. **Supporting Fig. S34**: In operando removal efficiency of 20 mL of 0.01 mM initial concentration of (a) MO and (b) T85 dye aqueous solution after 360 min in the dark and the presence of light under direct photolysis, pristine silica and 700 cycles TiO_{2-x} ultrathin films coated-silica annealed (500°C) under forming gas (5%H_2/95%Ar). **Supporting Fig. S35**: The negative logarithmic plot of L-H photodegradation kinetics due to 700 cycles of TiO_2 films coated-QFF on (a) MO and (b) T85 dye aqueous solution with an initial concentration of 0.01 mM after 360 min. **Supporting Fig. S36**: (a) UV–vis–NIR transmittance (%) of polycarbonate sheet (10 mm) and (b) UV unfiltered and filtered simulated light intensity (metal halide lamp) used during the photocatalytic experiment tests. **Supporting Table S1**: Annealing temperature range. **Supporting Table S2**: RTA voltage settings versus achieved annealing temperatures. **Supporting Table S3**: XRR film thickness as a function of annealing temperatures. **Supporting Table S4**: Band gaps of the as-deposited TiO_2 and TiO_{2-x} ultrathin films. **Supporting Table S5**: Kinetic parameters evaluated during photodegradation of MO and T85 using TiO_2 films coated-QFF as a function of annealing temperatures. **Supporting Table S6**: Calculated turnover numbers of dye molecules degraded to the number of TiO_2 molecules due to photocatalytic degradation of MO and T85 with as-deposited (250°C) TiO_2 thin films coated onto silica substrates. Note that the number of TiO_2 molecules for the TiO_{2-x} samples were assumed to be the same as for the TiO_2 (anatase) sample. **Supporting Table S7**: Calculated turnover numbers of dye molecules degraded to the number of TiO_2 molecules due to photocatalytic degradation of MO and T85 with annealed TiO_2 and TiO_{2-x} films (700 cycles) coated onto silica substrates under MH-full spectrum. Note that the number of TiO_2 molecules for the TiO_{2-x} samples were assumed to be the same as for the TiO_2 (anatase) sample. **Supporting Table S8**: Estimated AQY due to photocatalytic degradation of 0.01 mM MO and T85 dye molecules using stoichiometric as-deposited (200°C, 11.9 – 28.05 nm) TiO_2 (300 – 700 cycles) thin films under MH- full spectrum. Note that the number of TiO_2 molecules for the TiO_{2-x} samples were assumed to be the same as for the TiO_2 (anatase) sample. **Supporting Table S9**: Estimated to photocatalytic degradation of 0.01 mM MO and T85 dye molecules using stoichiometric annealed (300 – 1100°C) 700 cycles TiO_2 and sub-stoichiometric TiO_2 (TiO_{2-X}) thin films. The light sources employed were either i) the full spectrum of the MH lamp; ii) the filtered spectrum of the MH lamp (λ > 400 nm); or iii) the UV-LED (365 nm). Note that the number of TiO_2 molecules for the TiO_{2-x} samples were assumed to be the same as for the TiO_2 (anatase) sample.